# ABSTRACT

| | |
|---|---|
| Title of Thesis: | CONTACTLESS SPECTRAL-DEPENDENT MEASUREMENT OF BULK LIFETIME AND SURFACE RECOMBINATION VELOCITY IN SILICON PHOTOVOLTAIC MATERIALS |
| | John Frederick Roller, Master of Science 2016 |
| Thesis Directed By: | Dr. Mario Dagenais, ECE |

Charge carrier lifetime measurements in bulk or unfinished photovoltaic (PV) materials allow for a more accurate estimate of power conversion efficiency in completed solar cells. In this work, carrier lifetimes in PV- grade silicon wafers are obtained by way of quasi-steady state photoconductance measurements. These measurements use a contactless RF system coupled with varying narrow spectrum input LEDs, ranging in wavelength from 460 nm to 1030 nm. Spectral dependent lifetime measurements allow for determination of bulk and surface properties of the material, including the intrinsic bulk lifetime and the surface recombination velocity. The effective lifetimes are fit to an analytical physics-based model to determine the desired parameters. Passivated and non-passivated samples are both studied and are shown to have good agreement with the theoretical model.

# CONTACTLESS SPECTRAL-DEPENDENT MEASUREMENT OF BULK LIFETIME AND SURFACE RECOMBINATION VELOCITY IN SILICON PHOTOVOLTAIC MATERIALS

by

John Frederick Roller

Thesis submitted to the Faculty of the Graduate School of the
University of Maryland, College Park, in partial fulfillment
of the requirements for the degree of
Master of Science
2016

Advisory Committee:
Professor Mario Dagenais, Chair
Professor Martin Peckerar
Dr. Behrang Hamadani

© Copyright by
John Frederick Roller
2016

# Acknowledgements

I would like to thank my NIST advisor, Dr. Behrang Hamadani, for his guidance and encouragement, for the passionate way in which he approaches research, and for always making himself available for any issues that arose. I would also like to thank my UMD advisor, Prof. Mario Dagenais, for his advice and feedback which kept me on track. Also, thank you to my supervisor Dr. Bill Healy who helped to provide the opportunity and resources to make this work possible.

I would like to thank the rest of my coworkers in the Energy and Environment Division at NIST for their support and for creating an enjoyable work environment.

Finally, I would like to thank my parents, Tom and Donna, and my sister Casey for their full support and encouragement.

# Table of Contents

Acknowledgements ..... ii
Table of Contents ..... iii
Introduction ..... 1
Chapter 1: Background ..... 4
1.1 Charge Carriers in Semiconductors ..... 4
1.1.1 Band Structure in Semiconductors ..... 4
1.1.2 Fermi Energy Levels and Doping ..... 7
1.1.3 Excess Carriers and Quasi-Fermi Levels ..... 8
1.2 Carrier Transport ..... 9
1.2.1 Drift, Mobility, and Conductivity ..... 9
1.2.2 Diffusion ..... 11
1.2.3 The Continuity Equation ..... 11
1.3 Recombination Processes ..... 12
1.3.1 Shockley Read Hall Recombination ..... 12
1.3.2 Auger Recombination ..... 14
1.3.3 Radiative/Non-Radiative Recombination ..... 15
1.3.4 Surface Recombination ..... 16
1.3.5 Emitter Recombination ..... 17
1.4 Generation Processes ..... 18
1.4.1 Optical Generation ..... 18
1.5 Carrier Lifetime Measurement ..... 19
1.5.1 Bulk and Effective Lifetimes ..... 19
1.5.2 Quasi-Steady State Measurements ..... 20
1.5.3 Transient Measurements ..... 21
Chapter 2: Measurement and Analysis ..... 22
2.1 Eddy Current Conductance Measurement ..... 23
2.2 Conductance Measurement Technique ..... 26
2.3 LED Signal Input ..... 27
2.4 Input Signal Measurement Technique ..... 31
Chapter 3: Carrier Lifetimes in Silicon ..... 32
3.1 Calculation of Effective Lifetimes through Photoconductance ..... 32
3.1.1 Calculation of the excess carrier density ..... 33
3.1.2 Calculation of the generation rate ..... 35
3.1.3 Comparison of LED method with Current Measurement Techniques ..... 38
3.2 Modeling of carrier concentrations and lifetimes ..... 40
3.2.1 Modeling of Depth Dependent Carrier Density ..... 40
3.2.2 Modeling of Spectral Dependence of Lifetime ..... 45
3.3 Corrections to Measurements ..... 47
3.3.1 Corrections for Photoconductive Traps ..... 48
3.3.2 Corrections for Pathlength Enhancement ..... 49
3.4 Measured Wafers and Analytical Model Fits ..... 50
3.4.1 Unpassivated 1mm thick n-type sample ..... 51

3.4.2 Unpassivated and Passivated n-type Wafers ........................................... 52
3.4.3 Unpassivated and Passivated p-type wafers ........................................... 53
3.5 Effects of Excess Carrier Densities ........................................... 54
Conclusions ........................................... 56
Bibliography ........................................... 57

# Introduction

Charge carrier lifetime is an important physical quantity of a semiconductor material. Knowledge of this quantity is not only useful in device design or architecture, but is also a very helpful tool for material quality diagnostics because a higher lifetime generally correlates with a higher purity material.[1]–[3] In thinner materials, or semiconductor wafers where the intrinsic charge carrier lifetimes are high enough so that the corresponding diffusion length is on the order of the device thickness or smaller, the surface effects can play a dominant role on the measured *effective* charge carrier lifetime.[4] When a wafer is not properly passivated on both sides, the surface recombination velocity is very high. Under these conditions a very high-quality, high-bulk lifetime material will show very reduced effective lifetimes, making it difficult to understand if the bulk material is of high quality. The effective lifetime in silicon, however, has a spectral dependence because of the wavelength dependence of the absorption coefficient. This study sets out to investigate these effects by use of a light emitting diode (LED)-based technique coupled with a contactless RF photoconductance measurement apparatus. The LEDs, which come in a variety of wavelengths from 460 nm to 1032 nm and whose intensity and mode of operation can be controlled electronically, allow for determination of the spectral dependence of the lifetimes over a large excess carrier density range. The results can then be used to separate bulk properties from the surface effects.

Previous techniques to measure the surface recombination velocity and bulk lifetime usually consist of a two beam measurement consisting of a photogenerating pump beam and an IR probe beam. The pump beam consists of photons above the bandgap

energy of the material that will be absorbed and the probe beam consists of photons below the bandgap energy that will transmit through the material. Deflections and changes in the intensity of the probe beam are caused from the excess carriers generated from the pump beam allowing for a measurement of the lifetime.[5]–[8]

In addition to the pump-probe method, microwave photoconductivity decay (μPCD) has also been used to characterize wafers. This process involves measuring the reflected power of incident microwaves, which is proportional to excess charge carrier concentration. [9]–[11]

In this study, the lifetime will be measured in a different way. The conductivity of the wafer under illumination will be used in order to determine the excess carrier concentration, and changes in the spectral profile of the incident photons will allow for a determination of bulk lifetime and surface recombination velocity. This measurement is based on an analytical model that relates the effective carrier lifetimes measured and the corresponding incident photon wavelengths to the bulk lifetime and surface recombination velocity of a wafer.[12], [13]

This thesis will first outline the mechanisms involved with charge carrier transport in silicon before covering the specifics related to the calculation of charge carrier lifetimes. After a general discussion of carrier transport, there will be an overview of the measurement apparatus used in order to measure the effective carrier lifetimes. An LED plate consisting of narrow bandwidth LEDs ranging from 460nm to 1032nm was used to generate the carriers at the various wavelengths so the spectral effects could be studied. A RF operated coil was coupled with the measured materials to

extract wafer photoconductivity, which was then used to calculate excess carrier concentration.

Following the description of the measurement apparatus, the data collected from the measured wafers will be discussed. Several samples were measured using this photoconductive measurement technique and were found to fit the spectral dependent model. Using this model, bulk lifetime and surface recombination data was extracted for samples at various stages of the solar cell production process.

# Chapter 1: Background

The research conducted for this thesis involves calculating the carrier lifetimes in silicon from a series of electrical and optical measurements.  This chapter will focus on the underlying physics used to describe the mechanisms at work within the material as well as covering the varying factors that are involved in charge carrier lifetimes.

## 1.1 Charge Carriers in Semiconductors

### *1.1.1 Band Structure in Semiconductors*

The structure of crystalline semiconductor materials such as silicon, germanium, or gallium arsenide is made up of several covalently bonded atoms which share their valence electrons.  At 0 K, all of these electrons are in their lowest possible energy states and all are located in valence energy states keeping them bound to the atoms. When thermal energy is added to the system and the lattice is at a temperature above 0K, there will be motion in the lattice and some electrons will be in a higher energy state where they are free to move throughout the material.  These electrons leave behind a hole when they are excited to this conduction state.  Through quantum physics using the Schrodinger Equation and Kronig Penney Model, it can be shown that these energy states can be represented by a valence band and a conduction band separated by an energy gap.[14] The energy gap, seen in Figure 1, separates the two energy state bands with the condition that no carriers can occupy energies within the energy gap.

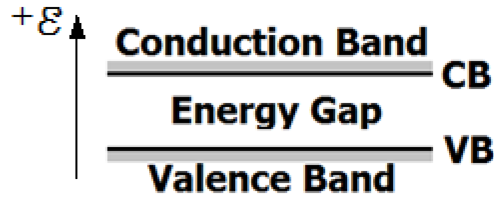


Figure 1: Representation of the semiconductor band structure. Resting electrons and conducting holes are held in the valence band. Resting holes and conducting electrons are held in the conduction band.

The concentration of electrons and holes within the conduction or valence band is dependent on the temperature as well as other properties of the material. These properties include the effective electron and hole masses, or altered mass values for the carriers which help explain their inertia within the lattice. The carrier distribution between the two bands can be explained using Fermi-Dirac distribution about the intrinsic Fermi energy of the material.

The Fermi energy of a material is based on the concentration of electrons and holes in the conduction or valence band. For an intrinsic or pure material, there are as many electrons as holes in conduction states. This causes the Fermi energy to be very close to the center of the energy gap, however it is not necessarily in the exact center. Depending on the density of allowed energy states in both the conduction and valence bands, the carrier distribution within the bands is not necessarily the same. The density of energy states is a function of the effective mass of the electrons in the conduction band and that of holes in the valence band. The intrinsic Fermi energy, $E_{Fi}$, of a material can be calculated by Equation (1) where $m_p^*$ and $m_n^*$ are the effective masses of holes and electrons, respectively. In this equation $k$ is the Boltzmann constant and $T$ is the absolute temperature of the material.

$$E_{Fi} = \frac{1}{2}(E_C - E_V) + \frac{3}{4}kT\ln\left(\frac{m_p^*}{m_n^*}\right) \tag{1}$$

The equilibrium concentration of electrons in the conduction band and holes in the valence band of a material can then be calculated using Equations (2) and (3). The intrinsic density of electrons, $n_i$, is calculated using the density of states in the conduction band, $N_C$, as well as the Fermi and conduction band energies. The intrinsic density of holes is calculated based on the properties of the valence band.

$$n_i = N_C \exp\left[\frac{-(E_C - E_{Fi})}{kT}\right] \tag{2}$$

$$p_i = N_V \exp\left[\frac{-(E_{Fi} - E_V)}{kT}\right] \tag{3}$$

The density of states values for these equations are calculated based on physical constants and can be seen in Equations (4) and (5).

$$N_C = 2\left(\frac{2\pi m_n^* kT}{h^2}\right)^{\frac{3}{2}} \tag{4}$$

$$N_V = 2\left(\frac{2\pi m_p^* kT}{h^2}\right)^{\frac{3}{2}} \tag{5}$$

Since there are equal amounts of intrinsic holes and electrons, Equations (2) and (3) can be combined to show that the intrinsic carrier concentration is not dependent on the intrinsic Fermi energy, but is dependent on the size of the energy gap, $E_g$. This is shown in Equation (6).

$$n_i^2 = N_C N_V \exp\left[\frac{-E_g}{kT}\right] \tag{6}$$

*1.1.2 Fermi Energy Levels and Doping*

The concentration of electrons and holes can vary from the intrinsic values through doping the crystal with various atoms. Usually this is done by having an impurity in the lattice. These impurity atoms will contribute to extra electrons in conduction band states (donors) or extra holes in the valence band states (acceptors). For silicon, common dopants include Boron, Phosphorus, Arsenic, and other Group III or V elements. It should be noted that while these dopant atoms add a mobile charge into the material, the material remains charge neutral.

Dopants will shift the equilibrium amounts of electrons and holes in the material causing the equilibrium Fermi energy to shift from its intrinsic value near the middle of the gap. The equilibrium concentration of carriers for the doped, or extrinsic, semiconductor can be calculated in a similar way to the intrinsic case, except the extrinsic concentrations $n_0$ and $p_0$ are based on the new Fermi energy, $E_F$. This is shown for electrons in Equation (7) which also shows the relation between the extrinsic and intrinsic concentrations $n_0$ and $n_i$.

$$n_0 = N_C \exp\left[\frac{-(E_C - E_F)}{kT}\right] = n_i \exp\left[\frac{E_F - E_{Fi}}{kT}\right] \tag{7}$$

Using equation (7) and its hole equivalent, it can be shown algebraically that the extrinsic semiconductor in thermal equilibrium follows equation (8).

$$n_0 p_0 = n_i^2 \tag{8}$$

Also from equation (7) it can be seen that adding donor dopants, which will increase the equilibrium amount of electrons, causes the Fermi energy to be higher, or closer to the conduction band edge, than the intrinsic value. Materials doped this way are referred to as n-type materials because the majority of carriers are negative charges,

or electrons. Conversely, adding acceptor dopants increases the equilibrium amount of holes and pushes the Fermi energy closer to the valence band edge. Materials doped this way are p-type materials because charge transport occurs mainly through holes, or positive charges in the valence band. If a material is doped so heavily that the Fermi energy is in one of the bands, the material is referred to as degenerately doped. This happens in n-type materials when the donor density is greater than the density of states in the conduction band and in p-type materials when the acceptor density is greater than the density of states in the valence band.

#### *1.1.3 Excess Carriers and Quasi-Fermi Levels*

In addition to doping, the amount of electrons and holes in the bands can be altered through energy absorption processes. Electrons can be excited up from the valence band to the conduction band through the absorption of photon energy. This excited electron leaves behind a hole, and the electron hole pair can now move about the crystal. These carriers, known as excess carriers, appear in pairs and will modify the equilibrium electron and hole densities by the same magnitude. The electron and hole densities in the material are represented in Equations (9) and (10) below. Since the excess electrons, $\Delta n$, are equal to the excess holes, the term $\Delta n$ is used in the hole equation as well.

$$n = n_0 + \Delta n \tag{9}$$

$$p = p_0 + \Delta n \tag{10}$$

When a material has excess carriers flowing, it is no longer in thermal equilibrium. Due to this, there is no strict Fermi energy level in the material. However, quasi-

Fermi energy levels can be defined that relate to the non-equilibrium electron and hole concentrations. These quasi-Fermi levels are defined based on equations (11) and (12). It should be noted that the quasi-Fermi levels $E_{Fn}$ and $E_{Fp}$ do not overlap. The quasi-Fermi level for electrons, $E_{Fn}$, is closer to the conduction band than the extrinsic Fermi level, $E_F$. Similarly, the quasi-Fermi level for holes is closer to the valence band.[15]

$$n_0 + \Delta n = n_i \exp\left[\frac{E_{Fn} - E_{Fi}}{kT}\right] \tag{11}$$

$$p_0 + \Delta n = n_i \exp\left[\frac{E_{Fi} - E_{Fp}}{kT}\right] \tag{12}$$

## 1.2 Carrier Transport

To determine electrical properties of a material, it is essential to measure the carrier concentration. In order to do this well, it is important to understand the underlying mechanisms of how carriers move within a material, as well as the relations between the carrier concentrations and electrical properties of the material.

### *1.2.1 Drift, Mobility, and Conductivity*

The drift of carriers in a material is the movement of these carriers based on an electric field. The electric field can be either an external field such as a voltage applied across the material, or may be caused by formation of a junction with another material such as a metal. This section will discuss the different components of the drift current, represented in multiple ways by Equation (13). Namely the conductivity, $\sigma$, and the mobility, $\mu$, will be covered in more detail. Note that

Equation (13) is in terms of the current density, $J$, which is a measure of the current flowing through a cross sectional area of a material.

$$J_{n,drift} = qnv_d = qn\mu_n\mathcal{E} = \sigma\mathcal{E} \tag{13}$$

The mobility, a measure of how easily carriers move within a material, is a key aspect of the drift current. Mobility is defined as the proportionality constant relating the drift velocity, $v_d$, with an applied electric field, $\mathcal{E}$.

$$v_d = \mu_d\mathcal{E} \tag{14}$$

The drift mobility can also be represented as a relation to the mean scattering time, $\tau_e$ for electrons, and can be seen in Equation (15).

$$\mu_n = \frac{q\tau_e}{m_e^*} \tag{15}$$

The other variables in this equation are the charge of the electron, $q$, and the effective mass of the electron, $m_e^*$. A similar equation can be written for holes based on their mean scattering time and an effective mass within the lattice.

The mean scattering times, $\tau_e$ and $\tau_h$, and the effective masses for the excess carriers are all dependent on properties of the crystal lattice. The temperature of a material and the dopant density can both alter the mobility within the material.[16]

The conductivity, $\sigma$, is another important electrical property related to the drift current. It is defined in Equation (16) as a function of carrier concentration and mobility.

$$\sigma = q(\mu_n n + \mu_p p) \tag{16}$$

Because the conductivity and its inverse, called the resistivity, $\rho$, are easily measurable electrical properties of materials, this relation is used to find the carrier concentrations.

### *1.2.2 Diffusion*

In addition to drift, carriers will also diffuse through a material going from areas of high concentration to areas of low concentration. The diffusion current, shown in Equation (17), is based on the diffusion coefficient and the distribution of carriers. The diffusion coefficient, $D$, is a property of the material at a given temperature and has separate values for electrons and holes.[17]

$$J_{n,diff} = qD_n \nabla n \tag{17}$$

In silicon, the diffusion coefficient is around $36cm^2/s$ for electrons and around $12cm^2/s$ for holes at 300K.

The drift and diffusion currents can be combined to find the net current in the material. The drift-diffusion equations can be seen in Equations (18) and (19).

$$J_n = J_{n,drift} + J_{n,diff} = qn\mu_n \mathcal{E} + qD_n \nabla n \tag{18}$$

$$J_p = J_{p,drift} + J_{p,diff} = qp\mu_p \mathcal{E} - qD_p \nabla p \tag{19}$$

### *1.2.3 The Continuity Equation*

The continuity equation is important for relating the density of carriers in a material to the charge carrier lifetime. Shown in Equations (20) and (21), the continuity equations state that the change of carriers in a unit volume over time is based on the net current of carriers into that volume plus the carriers generated in the volume minus the carriers that recombine within that volume. This process is modeled in Figure 2. The recombination rate $\Delta n/\tau$ is a ratio of the excess carriers to their lifetime. This lifetime, $\tau$, is the statistical average amount of time the carrier spends in a conducting state before recombination.[18]

$$\frac{dn}{dt} = \frac{1}{q}\nabla J_n + g_n - \frac{\Delta n}{\tau_n} \tag{20}$$

$$\frac{dp}{dt} = -\frac{1}{q}\nabla J_p + g_p - \frac{\Delta n}{\tau_p} \tag{21}$$

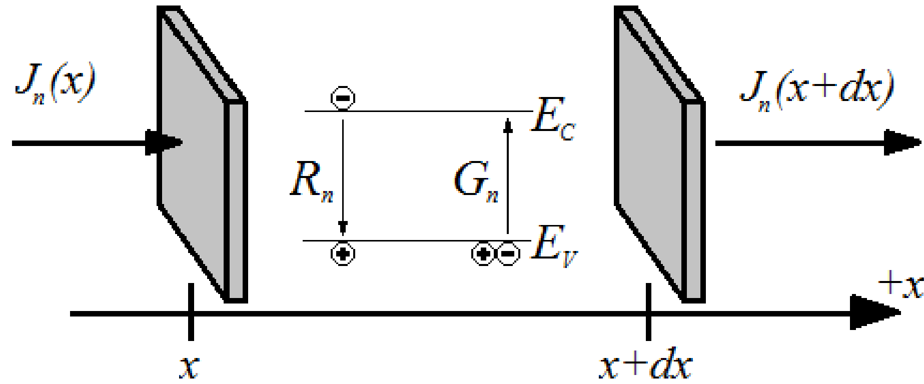


Figure 2: Representation of the variables in the one dimensional continuity equation. The change of electrons within the length x to x+dx is based on the net current into the length (based on the $J_n$ terms), recombination, $R_n$, and generation, $G_n$.

## 1.3 Recombination Processes

As stated in the previous section, the recombination of carriers depends on the amount of carriers in a material and the charge carrier lifetime. This lifetime consists of many factors and various recombination mechanisms alter the carrier lifetime in different ways. This section will discuss the prevalent recombination mechanisms for solar grade silicon.

### *1.3.1 Shockley Read Hall Recombination*

Shockley Read Hall (SRH) recombination is caused by imperfection states, or traps, in a semiconductor. These trap or defect states are often introduced into the material during the manufacturing process (such as iron impurities diffusing into silicon during the dicing of the wafers) and exist at energy levels between the valence band

and the conduction band.[19], [20] The recombination process occurs when a free electron in the conduction band or a free hole in the valence band gets captured by the trap state, and is therefore no longer freely flowing in the semiconductor. The trap state can reemit the trapped carrier, but then will be an empty state and can capture another carrier. This process can be seen in detail in Figure 3.

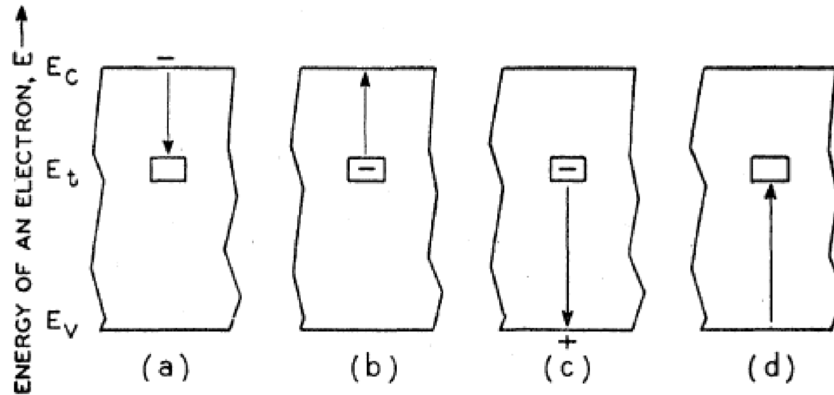


Figure 3: Representation of the Shockley Read Hall recombination processes through trapping. (a) and (b) represent electron capture and emission. (c) and (d) represent hole capture and emission. [21]

There are several of these trap states within the material and their influence on the overall recombination in the cell can be statistically modeled. The net recombination for this process is proportional to the number of majority carriers in the material, and can be seen through Equation (22).[21] The net rate of electron capture, $U_{cn}$, is dependent on several factors. These include the quasi Fermi levels of the traps, $E_{Ft}$, and electrons, $E_{Fn}$, the fraction of traps occupied by holes, $f_{pt}$, and a probability factor for an electron in the conduction band being trapped in the case where all traps are empty, $C_n$. Most importantly, the rate of electron capture is also proportional to the density of electrons in the conduction band, *n*.

$$U_{cn} = \left[1 - e^{\frac{E_{Ft}-E_{Fn}}{kT}}\right] f_{pt} n\, C_n \qquad (22)$$

Combining the other factors into fundamental electron and hole lifetimes, $\tau_{n0}$ and $\tau_{p0}$, the SRH recombination rate is given in Equation (23). The lifetime is based on the fundamental lifetimes, $\tau_{n0}$ and $\tau_{p0}$, the thermal equilibrium concentrations, $n_0$ and $p_0$, the concentrations that coincide with a Fermi level at the trap energy, $n_1$ and $p_1$, and the excess carrier concentration, $\Delta n$. [22], [23]

$$\tau_{SRH} = \frac{\tau_{n0}(p_0 + p_1 + \Delta n) + \tau_{p0}(n_0 + n_1 + \Delta n)}{n_0 + p_0 + \Delta n} \tag{23}$$

*1.3.2 Auger Recombination*

Auger recombination is a three carrier process by which the energy released by two carriers recombining is absorbed by the third carrier. Given this relationship the recombination rate can be seen in Equation (24). The low injection Auger coefficients, $C_n$ and $C_p$, are intrinsic parameters of crystalline silicon.[24], [25]

$$U_{Auger} = C_n n^2 p + C_p n p^2 \tag{24}$$

Under low injection conditions in n-type silicon, where $n$ is approximately the donor concentration, $N_D$, and $p$ is approximately $\Delta n$ with the condition $N_D \gg \Delta n$, this will cause the Auger lifetime to reduce to a constant value based on the doping of the material, as in Equation (25).

$$\tau_{Auger} = \frac{\Delta n}{C_n N_D^2 \Delta n + C_p N_D \Delta n^2} \approx \frac{1}{C_n N_D^2} \tag{25}$$

A similar lifetime can be found for p-type silicon based on the acceptor concentration. Under high injection conditions, where $n$ and $p$ are both approximately $\Delta n$, the Auger lifetime becomes carrier concentration dependent and can be reduced as in Equation (26).

$$\tau_{Auger} = \frac{\Delta n}{C_n \Delta n^3 + C_p \Delta n^3} \approx \frac{1}{C_a \Delta n^2} \quad (26)$$

The ambipolar Auger coefficient, $C_a$, is close to the sum of $C_n$ and $C_p$ but is generally larger. This is believed to be due to Coulomb enhancement where the formation of excitons increases Auger recombination. [26]

### *1.3.3 Radiative/Non-Radiative Recombination*

Radiative recombination is the inverse process of photon absorption in a semiconductor. This recombination is a two carrier process by which an electron and hole recombine and emit a photon. This recombination follows equation (27) where B is a radiative recombination constant.

$$U_{rad} = B\Delta n(N_D + \Delta n) \quad (27)$$

Using this recombination to find the radiative recombination lifetime gives Equation (28). From this equation the low injection lifetime is a constant value, but starts to fall off as $1/\Delta n$ as the injection level rises above a certain threshold.

$$\tau_{rad} = \frac{1}{B(N_D + \Delta n)} \quad (28)$$

For silicon, the value of B is very small because of its indirect band gap.[27] The radiative recombination process requires a phonon to conserve momentum between the carriers, causing the process to be more difficult than in a direct band gap semiconductor. Due to this, the intrinsic recombination processes in the material are dominated by the Shockley Read Hall effects for low injection and by Auger effects for high injection. This trend can be seen in Figure 4.

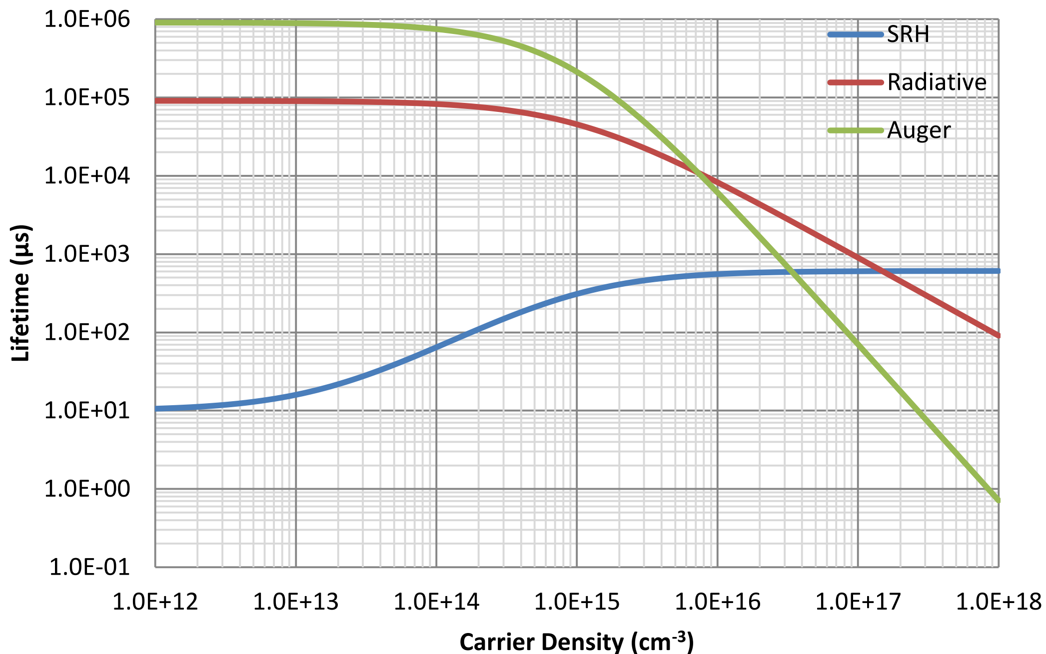


Figure 4: Comparison of the bulk recombination mechanisms in silicon. The dominant form of recombination is that with the lowest lifetime. Note how SRH is dominant in the low injection region and Auger is dominant in high injection.

### *1.3.4 Surface Recombination*

Surface recombination can be thought of as a specific type of Shockley Read Hall recombination that happens at the surfaces of a crystal structure. While the SRH recombination mentioned above involves a set of traps at a single energy level, the surface recombination involves traps at many levels within the bandgap.

Unlike other forms of recombination, surface recombination is analyzed based on a surface recombination velocity, $S$, instead of a lifetime value, $\tau$.[28]

For the analysis in this study, the surface recombination will be studied under steady-state like conditions, therefore it can be combined with the bulk lifetime as shown in Equation (29). This equation shows the simple combination of the bulk lifetime, due to the processes mentioned in the previous sections, with the surface recombination,

$S$, and the width of the sample, $W$. It is valid where the carriers can fully diffuse to the surfaces.

$$\frac{1}{\tau} = \frac{1}{\tau_{bulk}} + \frac{2S}{W} \tag{29}$$

The trap states that cause the surface recombination are caused by dangling bonds at the surface of the material where the crystal structure is no longer periodic. The silicon atoms that normally bond with four nearby silicon atoms no longer have sufficient atoms to bond with causing unpaired valence electrons.

The surface recombination can be significantly reduced through passivation processes that introduce atoms to the surface that reduce the number of unpaired valence electrons. This can be done through introducing hydrogen atoms to bond with the unpaired valence electrons, also known as hydrogen termination, or by depositing a thin layer of silicon nitride on the surface. The passivation process reduces the number of trap centers in the material causing the surface recombination to go down. [29]–[32] Passivation allows the bulk lifetime to have more of an effect on the overall lifetime of the material. Surface passivation is particularly important for very thin wafers.

### *1.3.5 Emitter Recombination*

Another form of recombination that can influence the effective lifetimes in solar cells is emitter recombination. This form of recombination deals with a highly doped, thin emitter region of the cell that will have its own set of recombination mechanisms.[33] In the high injection case, the recombination rate will be proportional to $\Delta n^2$ and at very high injection the emitter will have Auger effects proportional to $\Delta n^3$.

Excluding the Auger mechanisms, the emitter recombination can be represented as in Equation (30).

$$\tau_{emitter} = \frac{qn_i^2W}{2J_0(N_A + \Delta n)} \tag{30}$$

The low injection case is shown to be constant and dependent on the emitter saturation current density, $J_0$, and the emitter dopant density, $N_A$. The higher injection case is dependent on the excess carriers and falls off as $1/\Delta n$. [34]

## 1.4 Generation Processes

The processes in the previous section are mostly based on excess carriers, and these excess carriers need to be excited into a conduction state. This is done through a generation process where energy is absorbed by the carriers pushing them into a conducting state. The most common of these generation mechanisms is optical generation where light energy in the form of photons gets absorbed.

### *1.4.1 Optical Generation*

The optical carrier generation in photovoltaic materials is based both on properties of the material and properties of the incident light. As shown in Equation (31), the generation can be calculated using values for the absorption coefficient of the material, the incident photon flux, the transmittance, and the reflection of the material surface. [35] It is important to note that only photons with energy above the bandgap can be absorbed.

$$g = \int_0^W \int_{\lambda_{min}}^{\lambda_{max}} \alpha(\lambda)\phi(\lambda)e^{-\alpha(\lambda)x}\left(1 - r(\lambda)\right) d\lambda \, dx \tag{31}$$

The absorption coefficient, $\alpha$, for a material is dependent on the wavelength of the incident light and helps determine the amount of incident energy that is absorbed in the material. The incident photon flux, $\phi$, is a measure of how many photons are bombarding an area on the surface of the material. The transmittance is dependent on the depth into the material and is a measure of what proportion of the incident photons have reached the specified depth. The reflection, represented here by $1 - r$, takes into account the reflective properties of the front surface. The morphology of the surface also will refract the light entering the material, so the width over which the generation is calculated is a product of the actual width of the material and a path length enhancement factor.[36]

## 1.5 Carrier Lifetime Measurement

### *1.5.1 Bulk and Effective Lifetimes*

In looking at the several different types of recombination processes, it can be seen that specific lifetime curves can be produced as functions of excess carrier density. Each recombination process therefore has its own corresponding lifetime that can be calculated at any given carrier density. These lifetimes can be combined to form both the bulk and effective lifetime values which are more representative of a material as a whole.

The bulk lifetime corresponds to the combination of lifetimes that are intrinsic to the bulk crystal material. This would include such components as the Shockley Read Hall, Auger, and radiative/non-radiative lifetimes. The bulk lifetime will be

controlled by the dominant recombination mechanism, or shortest recombination, as shown in Equation (32).

$$\frac{1}{\tau_{bulk}} = \frac{1}{\tau_{\mathrm{SRH}}} + \frac{1}{\tau_{Auger}} + \frac{1}{\tau_{rad}} \tag{32}$$

In addition to the bulk lifetime which is important in modeling, there is another combination of lifetime values known as the effective lifetime. This is the value that can be obtained from physical measurements because it takes into account the surface states of the material.

$$\frac{1}{\tau_{eff}} = \frac{1}{\tau_{bulk}} + \frac{1}{\tau_{emitter}} + \frac{2S}{W} \tag{33}$$

*1.5.2 Quasi-Steady State Measurements*

Measurements of the effective lifetimes are done based on the continuity equation shown above in Equation (20). The lifetime measurement is done under equilibrium conditions making the current gradient term go to zero.[37] As such the lifetime can be expressed as shown in Equation (34).

$$\tau_{eff} = \frac{\Delta n}{g - \frac{d\Delta n}{dt}} \tag{34}$$

For the Quasi Steady-State (QSS) measurement of lifetime, the measurement is done under conditions where the temporal effect on the amount of excess carriers is negligible when compared with the generation rate, $g \gg \frac{d\Delta n}{dt}$. Therefore the effective lifetime of a sample can be calculated by using the amount of carriers in the sample and the generation rate in the material.

### *1.5.3 Transient Measurements*

The transient measurement of lifetime is also based on the continuity equation under equilibrium conditions. For the transient case, however, the generation rate in the sample is negligible when compared to the temporal effects, $\frac{d\Delta n}{dt} \gg g$. [37] For transient measurements, large amounts of excess carriers are generated using a pulsed source such as a flashlamp, and the lifetime can be found solely by measuring the amount of excess carriers as a function of time.

# Chapter 2: Measurement and Analysis

This section discusses the photoconductance and carrier generation measurements that contribute to the calculation of the carrier lifetimes for wafers. The measurement system is shown in Figure 5 and will be discussed in detail in this section.

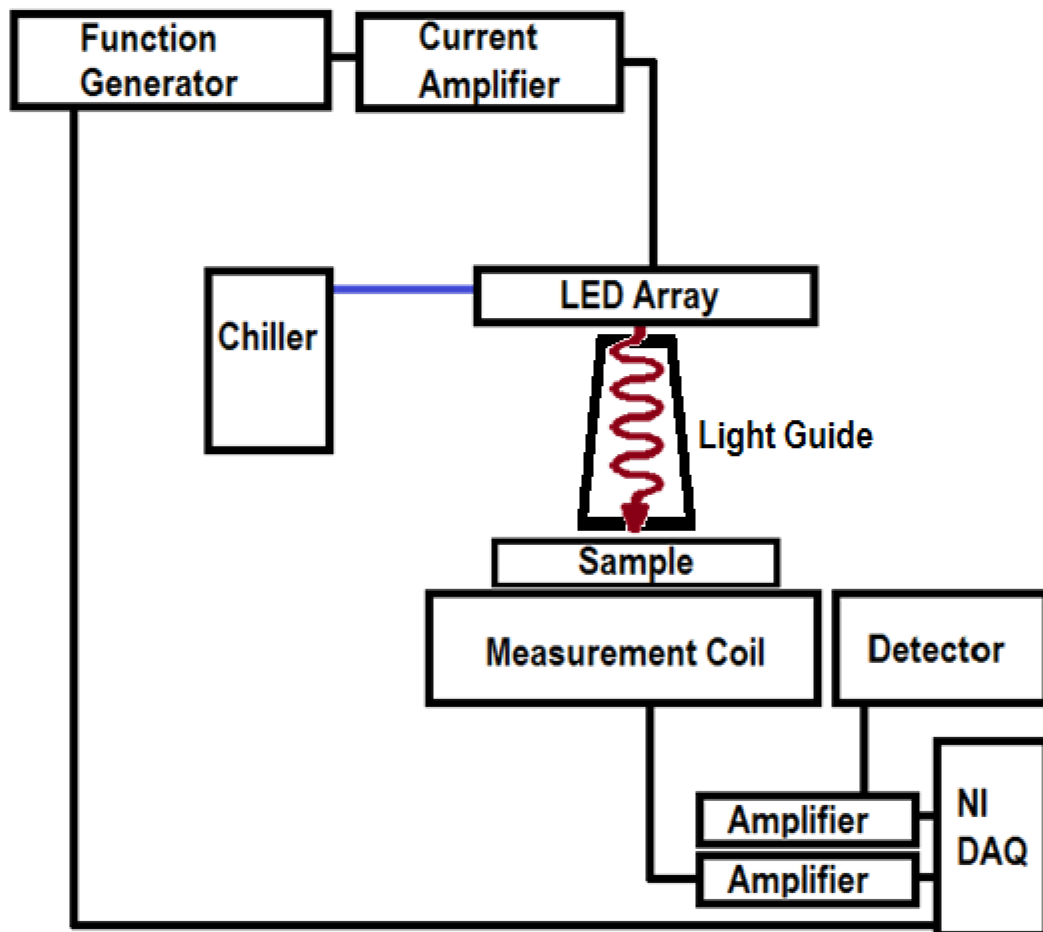


Figure 5:Schematic of the photoconductance lifetime measurement system. The LED array driving the lifetime measurement is run by a function generator coupled with a current amplifier and temperature controlled by a chiller. The measurement is done through a data acquisition system attached to a measurement coil and detector.

## 2.1 Eddy Current Conductance Measurement

In order to measure the conductive properties of the wafers, a contactless conductance measurement is performed utilizing eddy currents within the material. A contactless measurement removes sources of inefficiencies and defects that would be caused from attaching contacts to the material to be measured.[38]

This eddy current measurement uses a coupled inductive coil placed within a mounting stage for wafers. This coupled inductive coil is part of a tank circuit shown in Figure 6 and allows for measurement of conductivity as follows.

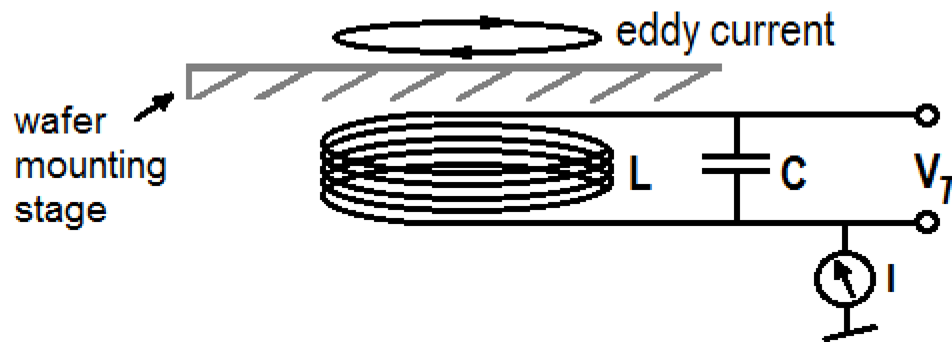


Figure 6: Coupled induction coil used in contactless conductivity measurement. Eddy currents are generated in wafers sitting on the stage due to the induction coil. The voltage across this tank circuit, $V_T$, is held constant due to feedback in a connecting oscillator circuit, and the current I can be shown to be proportional to the conductance of a mounted wafer.

The coil will generate a magnetic field, which will induce eddy currents in the nearby wafer. Assuming no losses due to flux leakage or skin effects, ohmic heating will cause some power absorption in the wafer. The power absorption is shown in Equation (35), where $V_T$ is the voltage across the tank circuit, $n$ is the number of turns in the coil, $\sigma$ is the conductivity of the coupled wafer, and $w$ is the wafer thickness.

$$P_{abs} = \frac{V_T^2}{8\pi n^2}\sigma w \tag{35}$$

The power across the coupled coil is given by Equation (36), where $I_{coil}$ is the current flowing through the induction coil.

$$P_{coil} = V_T I_{coil} \tag{36}$$

Combining these two power equations results in Equation (37), which shows that the current through the coil is proportional to the conductance of the coupled wafer.

$$I_{coil} = \frac{V_T}{8\pi n^2}\sigma w \tag{37}$$

Due to flux leakage and other loss mechanisms, the dependence of $I_{coil}$ on $\sigma w$ is not as strong as in Equation (37), but the relationship between the two variables is still linear and can be represented as in Equation (47) for coupling constant $K$.[39]

$$I_{coil} = K\frac{V_T}{n^2}\sigma w \tag{38}$$

Given an oscillator circuit with a feedback system that keeps $V_T$ constant, it can be seen that the driving current, $I_{coil}$, is proportional to the conductance, $\sigma$, of the wafer.[40] This driving current can be run through a resistor to get an output voltage from the oscillator circuit that is proportional to the wafer conductance. This output voltage, $V_{sig}$, is shown in Equation (39) where the physical constants are all combined into a coefficient, $C$.

$$V_{sig} = C\sigma t \tag{39}$$

This relationship can be used in conjunction with calibration wafers, or wafers with known conductivity values, in order to calibrate the instrument. In order to create a better fit for the measurement device, a single higher order coefficient is also used in the calibration which takes the form of Equation (40). [41] In this equation, $V_0$ is the

zero voltage, or the voltage given from the system with no wafer on the stage and $V$ is the measured voltage with the wafer present.

$$\sigma t = A(V - V_0)^2 + B(V - V_0) \tag{40}$$

This conductance measurement is also dependent on the thickness of the wafer. The response of the induction coil is dependent on the distance between the mounting stage and the conductive material. For instance, a wafer raised 1mm above the mounting stage would result in a lower voltage than if that same wafer was placed directly on the mounting stage. This spatial effect must be taken into effect for thicker wafers in order to obtain a correct conductance value. The correction for this effect can be seen in Equation (41) [42]

$$\sigma_{act}(x) = \sigma_{sense}(x)\, e^{\frac{x}{x_{sense}}} \tag{41}$$

The actual conductance of a material at distance $x$ away from the mounting stage, $\sigma_{act}(x)$, is related to the measured conductance, $\sigma_{sense}(x)$, multiplied by an exponential factor based on distance and a calculated sense depth, $x_{sense}$. This sense depth is a characteristic property of the coil and can be measured using several similar wafers stacked on top of one another. Figure 7 shows the measurement process by which the sense depth is calculated. Note how adding additional wafers of equal conductivity results in diminishing voltage differentials as the wafers get further and further away from the stage.

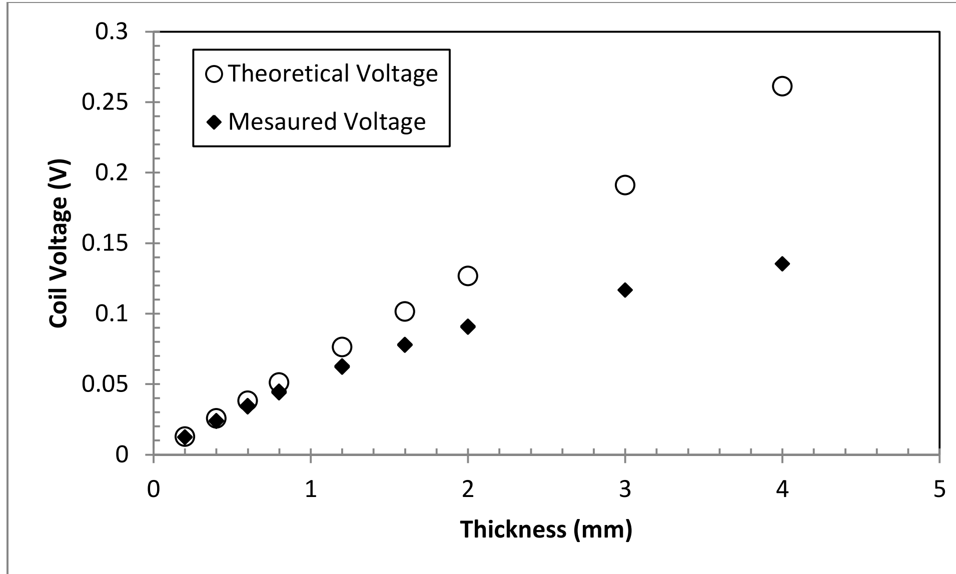


Figure 7: Voltage output of the Sinton WCT 120 Stage with several similar wafers stacked on the stage. The theoretical voltage represents the voltage which corresponds to the actual conductance of the wafers sitting on the stage, $\sigma_{act}$. The measured voltage is the signal being read by the coil which corresponds to $\sigma_{sense}$. The ratio of these two signals increases exponentially with thickness.

## 2.2 Conductance Measurement Technique

The measurements done in this study are based on the measurements done with the Sinton WCT120 system. This system uses a flashlamp in order to excite carriers for both transient and quasi-steady state (QSS) cases. The flashlamp can be set to different exposure times, and has measurement limitations based on the bulk lifetime of the wafers being measured. The QSS mode can only measure effective lifetimes up to around $100\mu s$ and the transient mode can only measure lifetimes down to around $100\mu s$. The limit on the transient lifetimes is because in order to measure faster lifetimes, a sharp temporal profile is required for the light pulse, which a flashlamp is not able to provide. As will be described in detail in Chapter 3, the effective charge carrier lifetimes in this study were required to be steady-state lifetimes; therefore, there was a requirement for QSS measurements with a much

longer maximum limit on lifetimes. Furthermore, this effective lifetime needed to be measured for a variety of wavelengths of light to isolate spectral effects. In order to be able to measure under the QSS condition, a different light source was coupled with the measurement stage of the Sinton system. A plate of narrow bandwidth LEDs was developed that would produce ample illumination for the wafers. These LEDs can be controlled through a function generator that allows for any input light profile. The intensity of the illumination can also be controlled by the magnitude of current sourced through the LEDs. This allows for much slower changes in signal, and allows for the QSS measurement on wafers with very high lifetimes at a variety of unique wavelengths.

For several of the measurements, the input signal used was a sine input with a frequency of 9.7Hz. The ability to change this frequency helped when transient effects became significant. The frequency could be lowered, causing these effects to play a less significant role.

## 2.3 LED Signal Input

The LED plate and coupled light guide system was developed for this measurement to provide ample illumination for several different wavelengths. Pictured in Figure 8, the LED plate consists of 13 LEDs, some of which are duplicates in order to increase the illumination for the shorter wavelengths where the photoconductance signal from the RF coil circuit is weaker. Two different LED suppliers were used for this experiment because all of the desired wavelengths were not available from a single vendor. In Figure 8, the two LEDs shown on the left (961nm and 1032nm) have

contact pins that go through the water-cooled plate and are wired from the back side, whereas the rest of the LEDs are surface mounted onto a custom designed PCB.

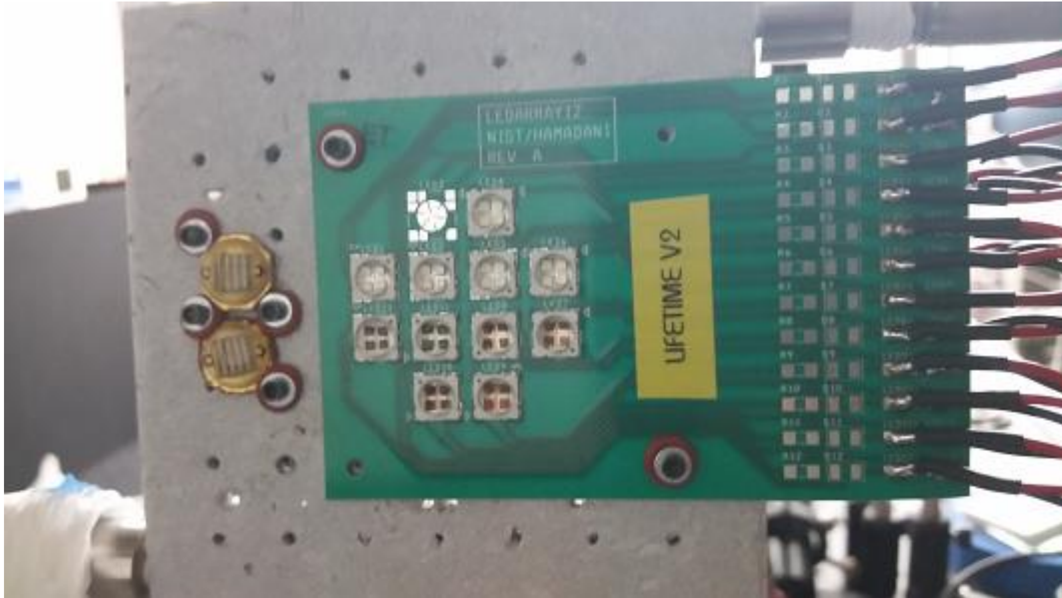


Figure 8: LED plate used for the lifetime measurements. This array consists of two 460nm, three 523nm, two 623nm, and one each of 660nm, 740nm, 850nm, 940nm, 961nm, and 1032nm LEDs. These LEDs are all mounted on a cooling plate to prevent overheating and reduce thermal effects.

These LEDs all have a relatively narrow bandwidth. LEDs were chosen for this measurement because they provided sufficient power and a narrow enough band to produce the spectral dependent results desired. The LED plate was also held at a constant 15°C using a water cooled mounting plate, allowing for repeatable output signals.

In conjunction with the LEDs, a high quality polished quartz light guide was used to focus the output signal. The LEDs emit diffuse light and in order to maximize the amount of output signal reaching the surface of the wafer to be measured, the light guide was used. This light guide and a schematic showing the internal reflections can be seen in Figure 9.

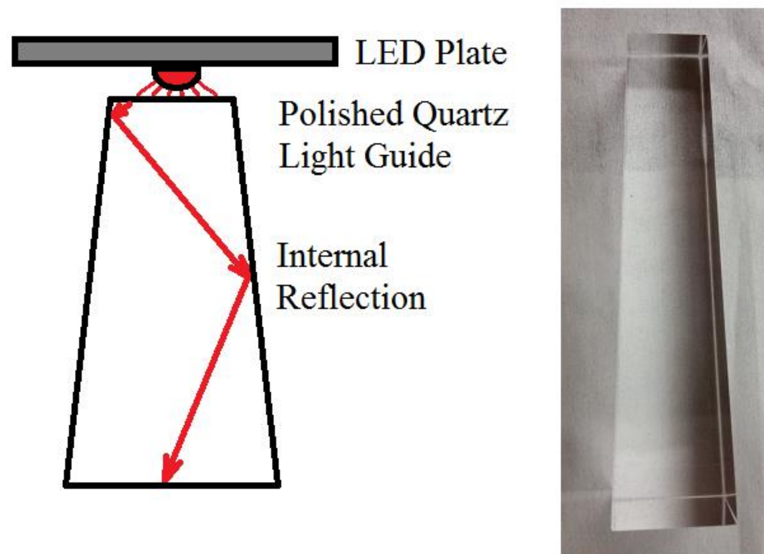


Figure 9: Polished quartz light guide used to direct light from the LEDs to the wafer to be measured. The light guide (right) internally reflects the diffuse light from the LED as shown in the diagram (left) so that it hits a wafer placed below the guide.

The polished quartz has very good reflective properties. Figure 10 shows the effect of shining a diffuse light through the light guide, and it can be seen that negligible light escapes through the sides of the light guide.

Figure 10: Demonstration of the internal reflections within the polished quartz light guide. Note how the diffuse light sourced on the left is redirected within the light guide and exits through the base located on the right.

Also, it should be noted that the light guide gives a uniform illumination over the large area required by the measurement coil (uniformity of better than 90%), a circle with about a 5cm diameter. The full measurement setup can be seen in Figure 11.

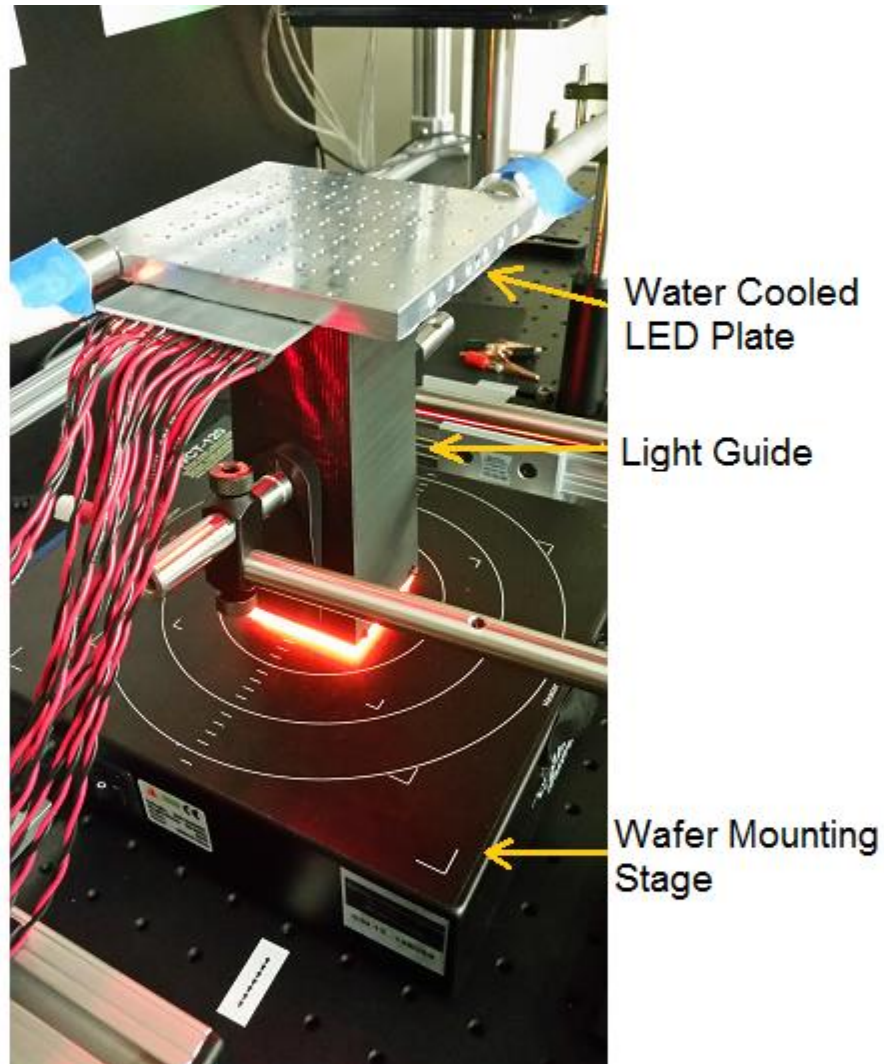


Figure 11: Measurement setup using the Sinton WCT120 base and the water cooled LED array with the light guide. The light guide is made from quartz and encased with a 3D printed holder. Note the uniform output of the LED array on the stage.

## 2.4 Input Signal Measurement Technique

For a proper measurement of the QSS lifetime it is also necessary to have an accurate measure of the generation of carriers within a wafer. In order to obtain this value, the input photon flux is measured with a calibrated photodetector. The response of the photodetector has been characterized by a responsivity curve. The current signal from the photodetector is then converted into an input intensity which gives the input photon flux. This flux is then used to calculate the generation rate based on the generation equation given in Equation (31) from Chapter 1. This process will be covered in more detail in Chapter 3.

# Chapter 3: Carrier Lifetimes in Silicon

This chapter will discuss the steps required to calculate the carrier lifetimes based on the input signals obtained from the measurement setup. First there will be a data comparison between this measurement system and the Sinton WCT-120 on a reference wafer. A discussion of the data from several PV grade silicon wafers will follow. The characterization of bulk lifetime and surface recombination velocity (SRV) using a spectral model is integral in the analysis of these wafers.

## 3.1 Calculation of Effective Lifetimes through Photoconductance

The measurement system described in Chapter 2 is used to acquire data from both the measurement coil and the reference detector. A sample output from the system can be seen in Figure 12.

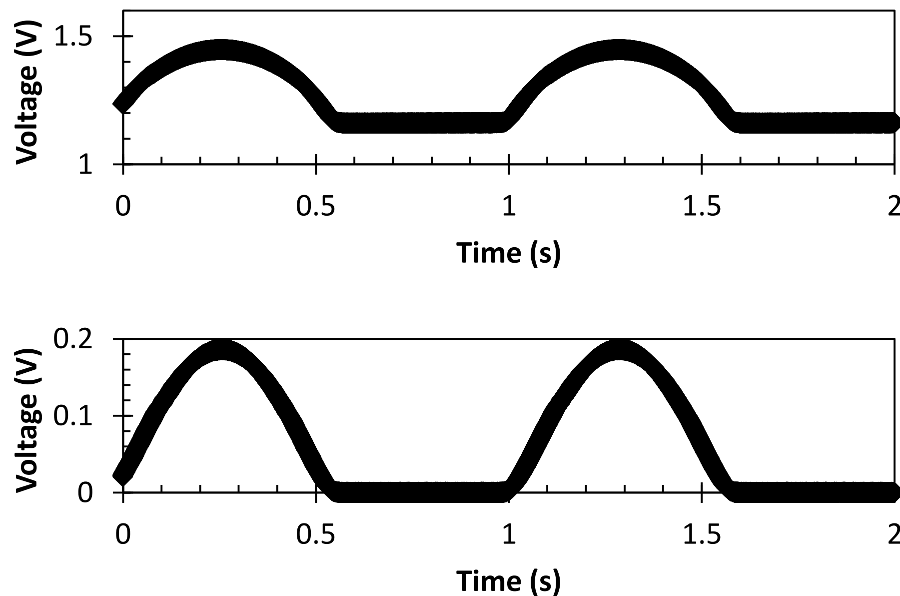


Figure 12: Output of measurement system. The photoconductive voltage from the coil (top) and the detector voltage (bottom) are measured from a wafer that was exposed to an LED sinusoidal pulsed light with an input 0.97 Hz frequency.

Note that the driving signal for the LED is a sine wave output from a function generator. This signal gets truncated based on a threshold voltage below which the LED is no longer on, resulting in the waveform seen. In the top curve, the flat part of the sine wave corresponds to the dark conductance of the wafer and is related to the dopant concentration of the material. A sine waveform input was chosen because any distortion to the signal due to transient effects could be easily noticed. These distortion effects did not occur at a frequency of 0.97Hz, but do occur when the input is at a high enough frequency, particularly when the charge carrier lifetime of the material is long.

These input signals are then modified based on the calculations in Chapter 2, and a more detailed discussion of the pieces involved follows next.

### *3.1.1 Calculation of the excess carrier density*

As can be seen in Chapters 1 and 2, the excess carrier density is a function of the photoconductance, which is itself a function of the voltage signal read by the induction coil. Equation (42) shows the algebraic combination of Equations (16) and (40) which is used to calculate the optically generated excess carrier density. In this equation the electron mobility, $\mu_n$, and hole mobility, $\mu_p$, are summed together to form a single mobility term, $\mu$.

$$\Delta n = \frac{\left(A(V - V_0)^2 + B(V - V_0)\right)e^{\frac{t}{t_{sense}}}}{q\mu t} \tag{42}$$

In order to obtain the value for the excess carriers, information about the constants in Equation (42) is needed. The mobility of electrons and holes in a material can be found based on the doping of the material, and is calculated as follows.

When finding the mobility values, first the bulk resistivity is calculated. This is done by taking two measurements from the system: one measurement of the system where no wafer is on the stage, $V_0$, and a second measurement where the wafer to be measured is on the stage in the dark, $V_{dark}$. The zero and dark voltage measurements are then used to calculate the resistivity of the wafer based on Equation (43).

$$\rho = \frac{t}{A(V_{dark} - V_0)^2 + B(V_{dark} - V_0)} \tag{43}$$

The resistivity is then used to find the doping density of the wafer, which is in turn used to find the mobility values for the wafer. This is calculated using an interpolation based on known values recorded for silicon. The data used for these interpolations can be seen in Figure 13.

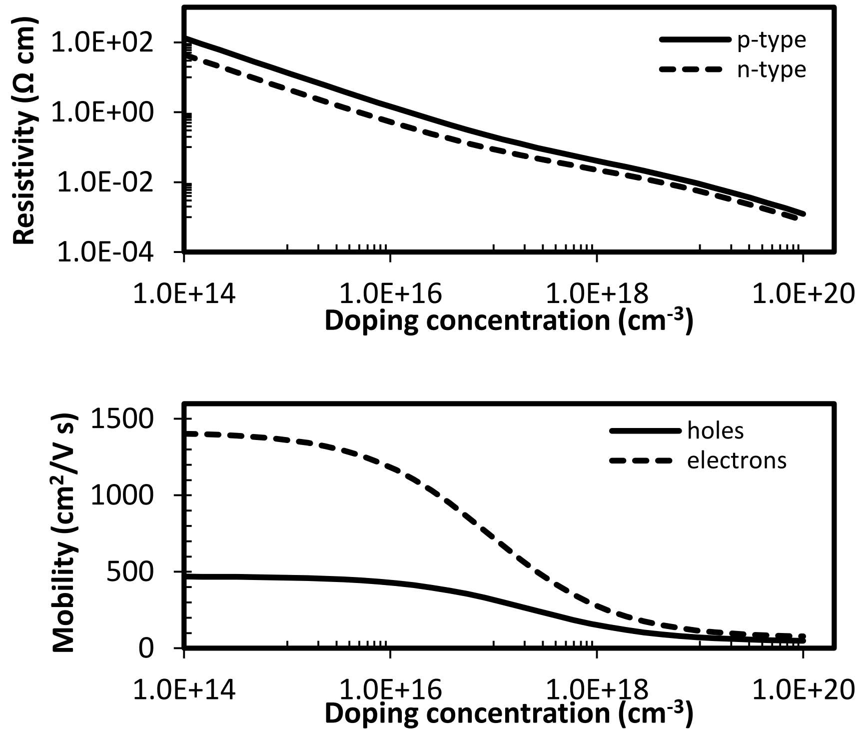


Figure 13: Resistivity (top) and mobility (bottom) as a function of doping concentration for silicon at 300K. The mobility values used in lifetime calculations are found by using the resistivity to calculate the doping concentration, and then using the doping concentration to get the mobility values.

Because the calculation for lifetime will be done based on the excess carriers, the excess electron and hole densities will be identical. Therefore the electron and hole mobilities are added together and this sum is used in calculations. A constant mobility is used for the calculations because the mobility was found to maintain a relatively constant value over the range of carrier densities measured.[43]

### *3.1.2 Calculation of the generation rate*

The second part of calculating the lifetime involves getting an accurate representation of the charge generation within the wafer. This is done by using measurements on the wafer, measurements on the LED input, and values for bulk silicon.

The generation rate is calculated based on Equation (31) which includes wavelength dependent variables such as the absorption coefficient, photon flux, and reflectance. The data used for the absorption coefficient was taken from a PC1D file for crystalline silicon at 300K. It can be seen in Figure 14 below.

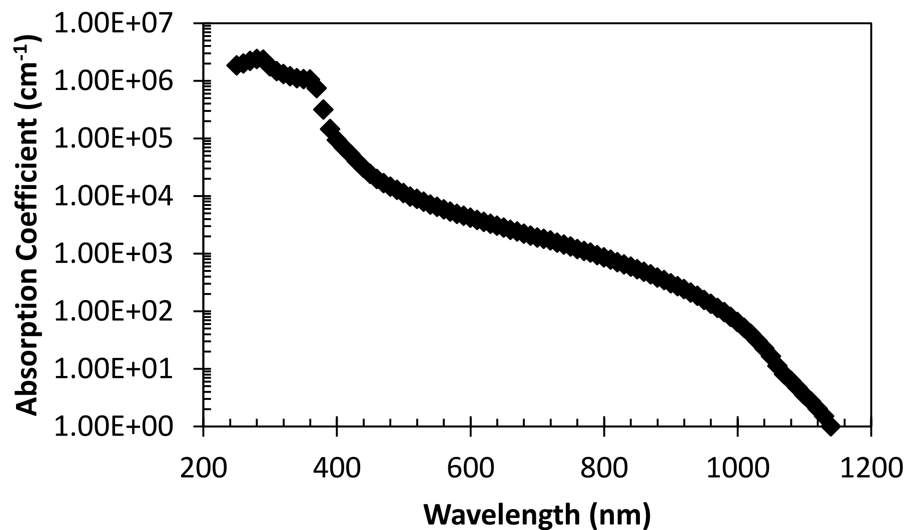


Figure 14: Absorption coefficients for crystalline silicon at 300K. These coefficients are used to calculate the generation in the measured wafers.

The reflectance was measured using a technique involving a monochromator and an integrating sphere. The monochromator would produce a varying monochromatic input signal incident on the wafer to be measured. Any light reflected off of the wafer will be trapped by the integrating sphere and will be read by a detector cell. The results of this measurement can be seen in Figure 15.

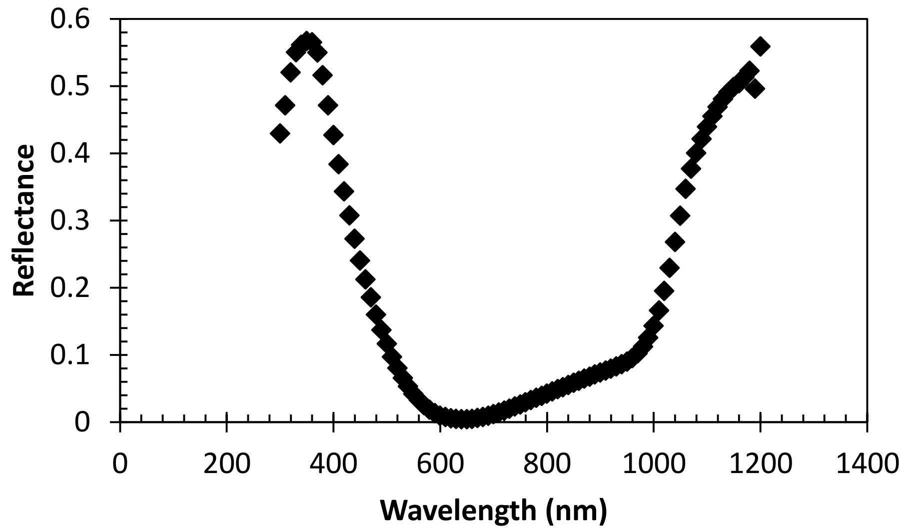


Figure 15: Measured reflectance of the Sinton reference wafer. Note that around 1000nm the reflectance rises due to reflections from the back surface of the material.

In addition to the absorption and the reflectance, the photon flux incident on the wafer also needs to be calculated. In order to do this calculation, a detector cell is used to obtain the incident irradiance from the LED and a spectroradiometer is used to obtain the spectral profile of the LED. The incident photon flux is related to the incident irradiance and the spectral profile as seen in Equation (44).

$$\phi(\lambda) = \frac{\hat{E}_{e,\lambda} V}{R(\lambda) G} \frac{\lambda}{hc} \tag{44}$$

The photon flux, measured in photons per second per unit area, is a function of the normalized spectral irradiance of the LED, $\hat{E}_{e,\lambda}$, the voltage measured by the photodetector, $V$, the responsivity of the detector, $R(\lambda)$, the gain of the

transimpedance amplifier connected to the photodetector, $G$, the wavelength, $\lambda$, Planck's constant, $h$, and the speed of light, $c$. The actual spectral irradiance of each LED was measured using a spectroradiometer. An integration was performed over the actual irradiance curve to calculate the integrated intensity for the LED. The actual irradiance was then scaled by the integrated intensity in order to get the normalized spectral irradiance curve, $\hat{E}_{e,\lambda}$. The normalized spectral irradiance of a 740nm LED can be seen in Figure 16 and the responsivity of the calibrated photodetector used in the measurements can be seen in Figure 17.

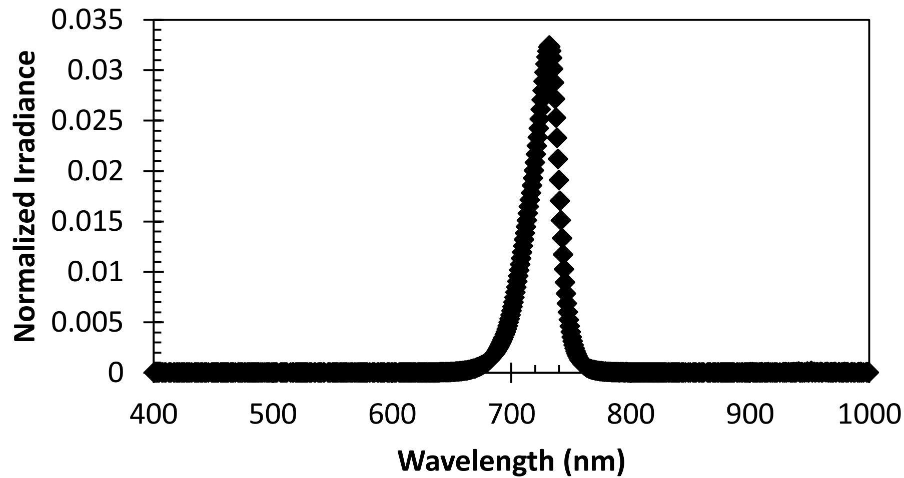


Figure 16: Normalized irradiance as a function of wavelength for a 740nm LED. The irradiance of the LED is calculated using a spectroradiometer and then normalized so that it can be scaled based on the measured input intensity.

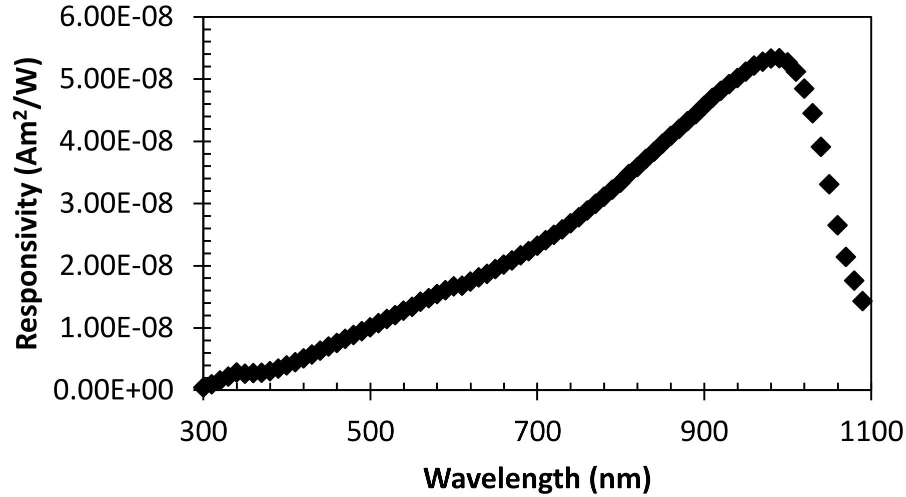


Figure 17: Responsivity of the calibrated detector cell. The measured reference voltage signal is converted into an input power based on the responsivity of the detector. A transimpedance amplifier converts the current out of the detector into the voltage measured, and the gain of the amplifier is also used in the input power calculation.

Substituting Equation (44) into Equation (31) from Chapter 1 gives Equation (45), which now represents the generation in terms of measured and calculated values for the wafer. This generation is then used with the carrier density calculated in the last section to calculate the effective lifetime in the wafer.

$$g = \int_0^w \int_{\lambda_{min}}^{\lambda_{max}} \alpha(\lambda) \frac{\hat{E}_{e,\lambda} V}{R(\lambda) G} \frac{\lambda}{hc} e^{-\alpha(\lambda)x} \left(1 - r(\lambda)\right) d\lambda \, dx \quad (45)$$

*3.1.3 Comparison of LED method with Current Measurement Techniques*

The measurement detailed in the previous section was validated by comparison to a similar measurement done with the calibrated Sinton WCT-120 system. The comparison between the two methods can be seen in Figure 18.

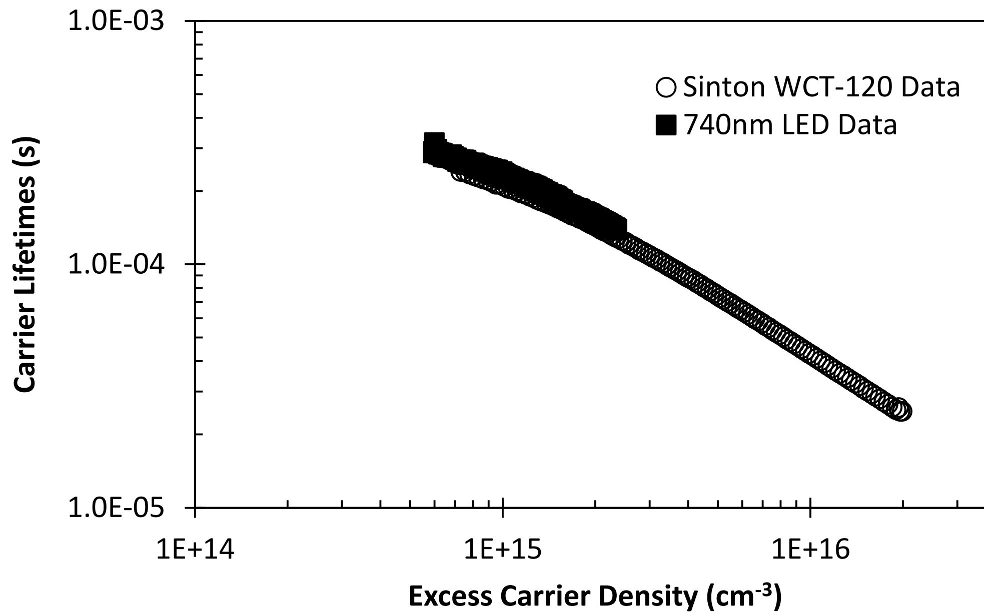


Figure 18: Comparison of lifetime data between the LED measurement system and the Sinton WCT-120 measurement system. Note that the LED system cannot reach the high carrier densities that the Sinton system can produce, but can probe low carrier densities.

The WCT-120 system uses a flashlamp to generate the carriers in a wafer placed on the stage. This flashlamp is placed in a way where it will also generate carriers in a photodiode placed within the stage. This simultaneous excitation of carriers in the wafer and photodiode generates the two signals needed to calculate the effective lifetime in the wafer. The flashlamp used is much more powerful than the LEDs but has temporal limitations as discussed in the previous chapter. It is also a broadband source, lacking the capability to perform wavelength dependent measurements. The WCT-120 measurement program calculates the lifetimes with inputs of the thickness of the wafer, resistivity, sample type, and an optical constant. This optical constant is an estimated value based on optical models and accounts for reflectance and transmittance effects.

As can be seen from Figure 18, the measurement system used in this thesis cannot generate as high of an excess carrier density as the Sinton WCT-120 system, however it can probe lower carrier densities. Slight differences in the calculated effective lifetimes measured can be attributed to nonuniformity in the wafer and potential sources of error in the WCT-120 measurement such as not having the correct optical constant. Differences in the light generation profile will not influence the lifetimes in this measurement because the reference wafer is well passivated. This effect will be covered in detail in Section 3.2.2.

## 3.2 Modeling of carrier concentrations and lifetimes

This section will discuss the various modeling work used to identify properties of the silicon wafers measured in this study. First, the drift-diffusion equations were used to calculate the steady state charge carrier density as a function of the depth within the wafer. This was used to verify the assumption that the carrier concentration was relatively constant through the wafer in the steady state case. Next the spectral effects on the effective lifetime were modeled. These effects are caused by higher wavelength photons penetrating further into the material, and in some cases some percentage transmitting through entirely. Last, there will be a discussion of modifications to the models based on surface texturing and other optical effects.

### *3.2.1 Modeling of Depth Dependent Carrier Density*

As described in previous chapters, the generation rate varies as a function of depth within a material. More photons will be absorbed near the front surface of the wafer than deep within the wafer due to absorption and transmission effects. The

photogenerated electrons and holes will diffuse through the material, and reach steady-state equilibrium. The purpose of this modeling is two-fold. First, it can be used to determine a representative carrier density and effective width of the material such that there will be one value for $\Delta n$ within the wafer. For thick wafers, the effective excess charge carriers, $\Delta n_{eff}$, will only be represented within an effective width, $w_{eff}$, outside of which the model assumes an excess carrier density of 0. $\Delta n_{eff}$ and $w_{eff}$ are defined in Equation (46) and Equation (47) respectively.[44], [45]

$$\Delta n_{eff} = \frac{\int_0^W \Delta n^2 dx}{\int_0^w \Delta n \, dx} \tag{46}$$

$$w_{eff} = \frac{\left(\int_0^W \Delta n \, dx\right)^2}{\int_0^W \Delta n^2 dx} \tag{47}$$

Second, the modeling based on one shorter and one longer wavelength reveals the distribution of the excess carrier density within the z direction under the influence of weak and strong surface effects. This will be explored in detail in Section 3.2.2. The model is based off of the diffusion equation, and is an algebraic combination of Equations (18) and (20) from Chapter 1. Since the wafer is assumed to be in steady-state, all temporal effects are reduced to 0. Also, the wafer is not subject to an external field so the drift current is also 0. This reduces the diffusion equation in one dimension to Equation (48), where the density of electrons, $n$, and the generation rate, $g$, are both functions of depth, $z$.

$$D \frac{d^2 n(z)}{dz^2} - \frac{n(z)}{\tau_{bulk}} = -g(z) \tag{48}$$

In order to numerically solve this model, a mesh of points is constructed evenly spaced in the $z$ direction, and boundary conditions based on the surface effects are added. These boundary conditions can be seen in Equations (49) and (50) where $S$ is the surface recombination velocity (assumed to be the same for both the front and back surfaces) and $W$ is the wafer thickness.[35], [46], [47]

$$D \frac{dn(z)}{dz}_{z=0} = S\,n(0) \tag{49}$$

$$-D \frac{dn(z)}{dz}_{z=W} = S\,n(W) \tag{50}$$

Figure 19 and Figure 20 show several runs of the numerical model with varying conditions for the bulk lifetime, $\tau_{bulk}$, the width, $W$, and the surface recombination velocity, $S$. For the purpose of meaningful comparison, the numerical simulations are performed in such a way that the total generation rate for each case is the same. Note how the effective carrier density is relatively close to the actual carrier density throughout the wafer. This shows that the recombination mechanisms at the effective carrier density are a good assumption for the recombination within the effective thickness. Also note that several of the models show an effective thickness lower than the modeled wafer thickness.

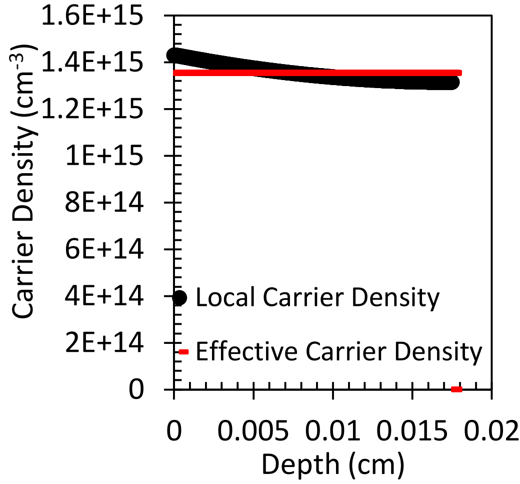


(a) Control
$\lambda = 523\text{nm}$, $W = 0.0175\text{cm}$
$S = 2\text{cm/s}$, $\tau_{bulk} = 150\mu\text{s}$
$\Delta n_{eff} = 1.35\text{E+15}$, $W_{eff} = 0.0175\text{cm}$

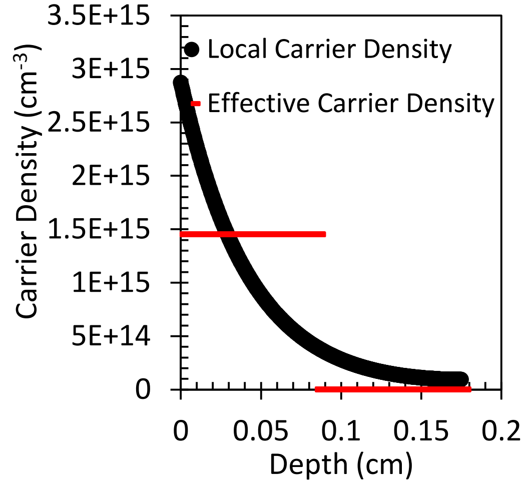


(b) Thick Wafer
$\lambda = 523\text{nm}$, $W = 0.175\text{cm}$
$S = 2\text{cm/s}$, $\tau_{bulk} = 150\mu\text{s}$
$\Delta n_{eff} = 1.45\text{E+15}$, $W_{eff} = 0.0844\text{cm}$

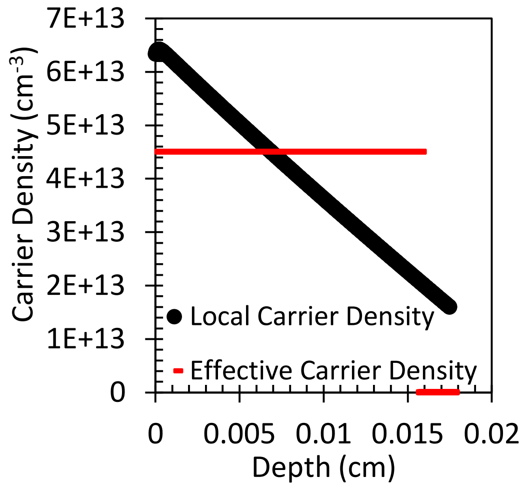


(c) High SRV
$\lambda = 523\text{nm}$, $W = 0.0175\text{cm}$
$S = 2000\text{cm/s}$, $\tau_{bulk} = 150\mu\text{s}$
$\Delta n_{eff} = 4.50\text{E+13}$, $W_{eff} = 0.0156$

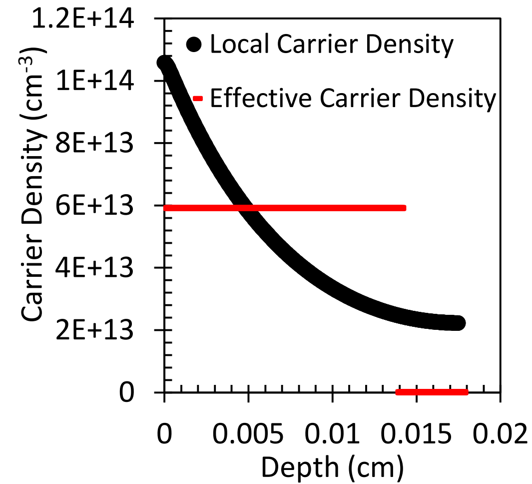


(d) Short Lifetime
$\lambda = 523\text{nm}$, $W = 0.0175\text{cm}$
$S = 2\text{cm/s}$, $\tau_{bulk} = 5\mu\text{s}$
$\Delta n_{eff} = 5.91\text{E+13}$, $W_{eff} = 0.0138\text{cm}$

Figure 19: Simulations of depth dependence of excess carriers in a silicon wafer. An input spectrum corresponding to an LED with effective wavelength 523nm was used to calculate the steady state responses shown. A control wafer with similar properties to a wafer used in this study was simulated, followed by altering values from this control to see the effects of increasing wafer thickness, increasing surface recombination velocity, and decreasing bulk lifetime.

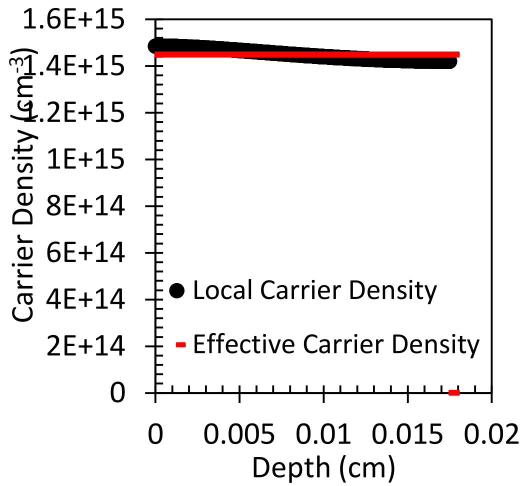


(a) Control Wafer
$\lambda = 940\text{nm}$, $W = 0.0175\text{cm}$
$S = 2\text{cm/s}$, $\tau_{bulk} = 150\mu\text{s}$
$\Delta n_{eff} = 1.45\text{E+15}$, $W_{eff} = 0.0175\text{cm}$

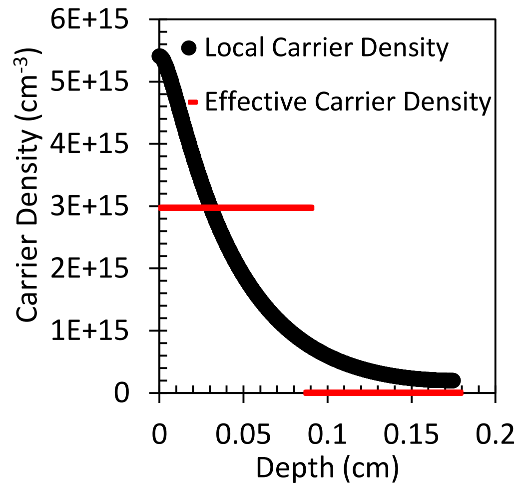


(b) Thick Wafer
$\lambda = 940\text{nm}$, $W = 0.175\text{cm}$
$S = 2\text{cm/s}$, $\tau_{bulk} = 150\mu\text{s}$
$\Delta n_{eff} = 2.97\text{E+15}$, $W_{eff} = 0.0863\text{cm}$

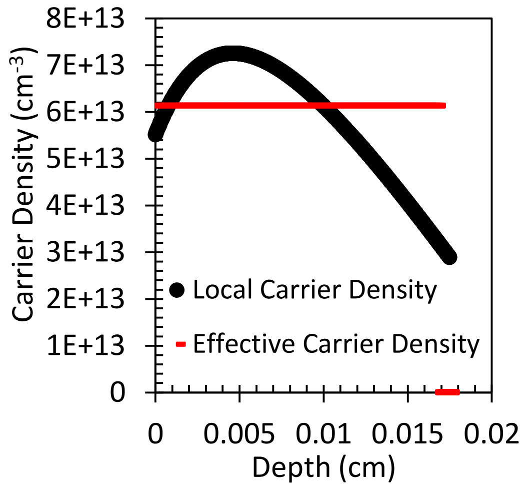


(c) High SRV
$\lambda = 940\text{nm}$, $W = 0.0175\text{cm}$
$S = 2000\text{cm/s}$, $\tau_{bulk} = 150\mu\text{s}$
$\Delta n_{eff} = 6.13\text{E+13}$, $W_{eff} = 0.0167\text{cm}$

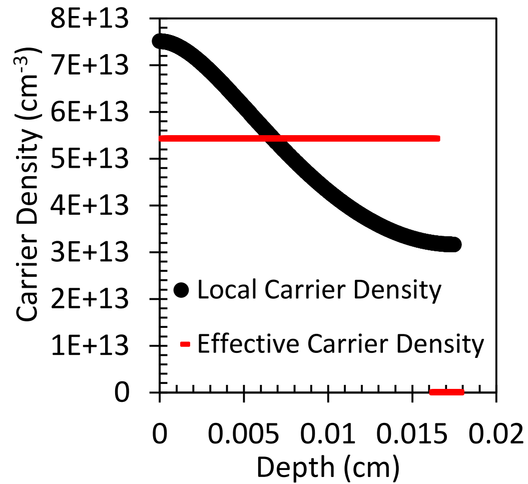


(d) Short Lifetime
$\lambda = 940\text{nm}$, $W = 0.0175\text{cm}$
$S = 2\text{cm/s}$, $\tau_{bulk} = 5\mu\text{s}$
$\Delta n_{eff} = 5.43\text{E+13}$, $W_{eff} = 0.0161\text{cm}$

Figure 20: Simulations of depth dependence of excess carriers in a silicon wafer. An input spectrum corresponding to an LED with effective wavelength 940nm was used to calculate the steady state responses shown. Similar to the previous figure, a control wafer with similar properties to a wafer used in this study was simulated, followed by altering values from this control to see the effects of increasing wafer thickness, increasing surface recombination velocity, and decreasing bulk lifetime.

*3.2.2 Modeling of Spectral Dependence of Lifetime*

As discussed in the previous section, the wavelength of the incident photons has an effect on how deep charge carriers are generated within a material. Figure 19 and Figure 20 demonstrate that the steady-state equilibrium of carriers is affected by the wavelength of the incident photons in the following manner: between the two control cases in Figure 19(a) and Figure 20(a) where $S$ is low, the calculated effective carrier densities are similar. This implies that the charge carrier lifetimes between the two wavelengths are relatively the same. However, in the cases shown in Figure 19(c) and Figure 20(c) where $S$ is high, a higher wavelength of light generates a larger $\Delta n_{eff}$. Furthermore, the distribution of carriers within the wafer is also affected by wavelength, with the peak carrier density deeper within the wafer for higher wavelength light. These numerical observations were recently explored by Marko Turek and were placed within an analytical framework that can better establish the connection between the modeled parameters. [12]

Using the same base diffusion differential equation as shown in Equation (48), a solution is found in the form of Equation (51). The value $l$ in this equation is the diffusion length and is defined as $l \equiv \sqrt{\tau_b D}$.

$$n(z) = c_1 e^{\frac{z}{l}} + c_2 e^{-\frac{z}{l}} + c_3 e^{\alpha z} + c_4 e^{-\alpha z} \tag{51}$$

The boundary conditions given in Equations (49) and (50) can be used to find the coefficients $c_{1-4}$. Equation (51) with determined coefficients and a generation equation given by Equation (52) are then used to calculate an effective lifetime according to Equation (53) where $W$ is the wafer thickness. In the generation

equation $P_\lambda$ is the illumination power, $A$ is the wafer area, and $r$ is the reflection coefficient.

$$g_\lambda(z) = \frac{\lambda P_\lambda}{Ahc}(1-r)\alpha e^{-\alpha z} \tag{52}$$

$$\tau_{eff} = \frac{\int_0^W n(z)dz}{\int_0^W g_\lambda(z)dz} \tag{53}$$

The analytical solution to this equation is found to be the wavelength dependent equation shown in Equation (54). [12]

$$\tau_{eff,\lambda} = \frac{\tau_b}{1-\alpha^2 l^2}\left[1 - \alpha l \; \frac{\alpha l + \frac{Sl}{D}\coth\frac{\alpha W}{2}}{1 + \frac{Sl}{D}\coth\frac{W}{2l}}\right] \tag{54}$$

This analytical solution shows that the effective lifetime at a specified wavelength, $\tau_{eff,\lambda}$, is a function of the bulk lifetime of the material, $\tau_b$, the wavelength dependent absorption coefficient, $\alpha$, the surface recombination velocity, $S$, the total width, $W$, the diffusion length, $l$, and the diffusion coefficient, $D$.

A plot of this analytical solution as a function of wavelength for the bulk lifetime, width, and surface recombination used in the control and high SRV plots in Figure 19 and Figure 20 can be seen in Figure 21. Note how the wavelength effects are more pronounced for the model with higher surface recombination, as described already. There are limitations on this model when either the bulk lifetime or surface recombination is dominant.[48]

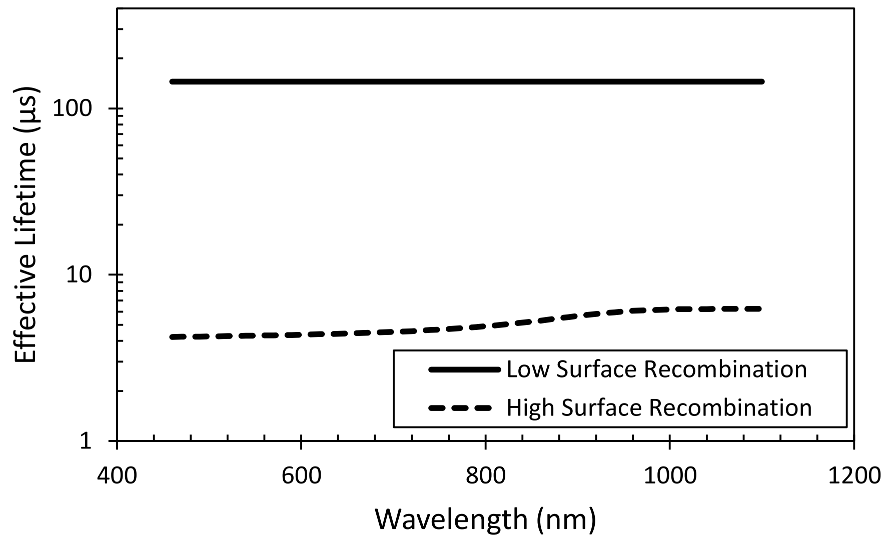


Figure 21: Modeled effective wavelengths for a wafer based on the analytical model calculated by Marko Turek. The values for bulk lifetime, surface recombination velocity, and wafer thickness are those used in the control and high SRV wafers of Figure 19 and Figure 20.

## 3.3 Corrections to Measurements

While the data analysis technique outlined in Section 3.1 was able to correctly calculate the lifetimes for the well passivated reference sample, other samples needed to be analyzed using a slightly altered method. For unpassivated samples, high trap densities led to an issue while reading the photoconductance of the wafers, particularly at the low light intensity conditions of the LED setup. In addition, for very thin samples, the use solely of the reflectance of the front surface did not fully capture the optical transmission through the wafer for wavelengths above 950nm. These two effects are explained in more detail in this section.

*3.3.1 Corrections for Photoconductive Traps*

It has been shown that photoconductive trap states can lead to a relatively large photoconductive response at a relatively low optical input. This effect, when left unaccounted for, causes the measured photoconductivity calculated to be artificially high and therefore the lifetime calculation would result in an incorrect value. This effect can be accounted for by using a bias term that subtracts out the photoconductive effects of the traps.[49]

The steady state response of one of the wafers measured as a function of input intensity can be seen below in Figure 22. The strong photoconductive response can be seen for input intensity below 10 $W/m^2$. In order to account for this large trap response, the slope of the carrier density vs generation rate curve is found in the region above a threshold generation rate. This slope is then used as the effective lifetime of the sample. The calculation of the effective lifetime from the slope is exemplified in Figure 23.

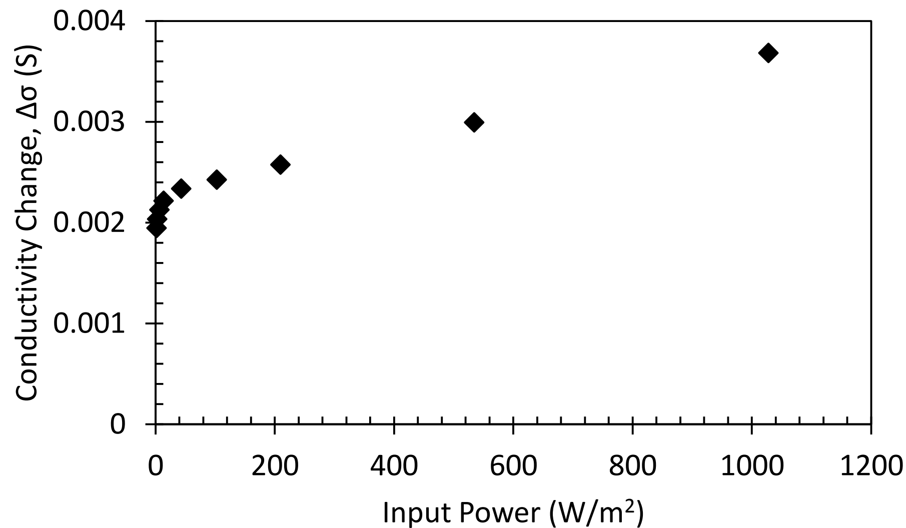


Figure 22: Measured conductive response of a 1mm n-type sample from a 940nm LED. Note that below an input power of $10W/m^2$, there is a rapid decline in conductivity. This is due to trap states in the wafer.

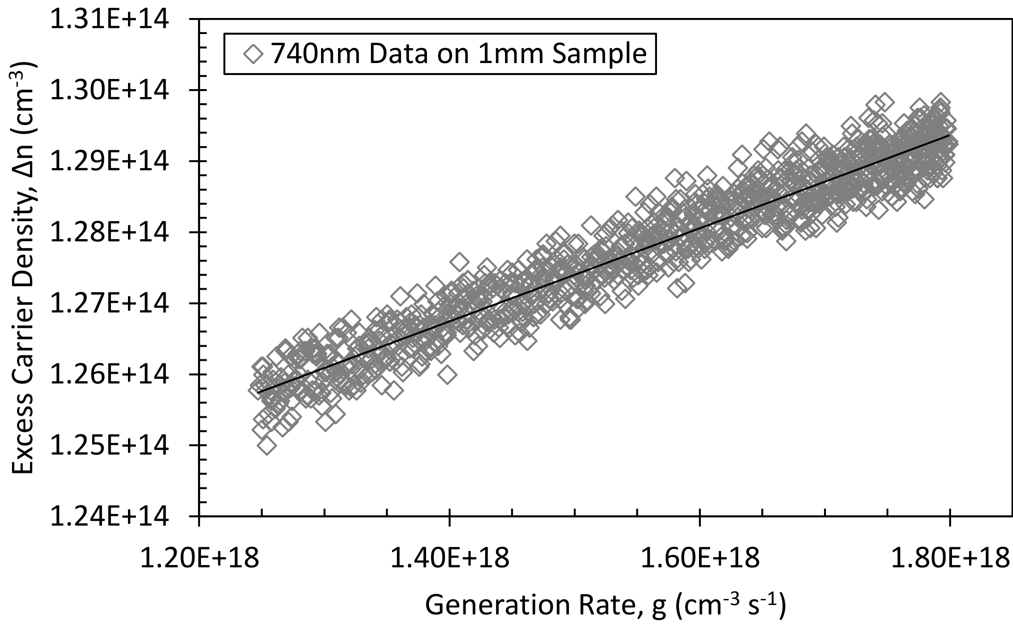

Figure 23: Excess Carrier Density vs Generation Rate curve for the 1mm sample with a 740nm LED input. The effective lifetime is calculated using the trendline through the measured data points. The equation for the trendline is given by $\Delta n = 6.56 \times 10^{-6}\, g + 1.18 \times 10^{14}$ giving an effective lifetime of $\tau_{eff} = 6.56\ \mu s$.

It should be noted that this correction can be used for all samples, but is especially important for the unpassivated samples measured in this study. This is due to the high trap concentration and low photoconductive response in these samples. Passivated samples such as the reference sample also show photoconductive trap effects, but they are minimal by comparison to the overall photoconductive signal generated.

### *3.3.2 Corrections for Pathlength Enhancement*

Through study of the surface morphologies of some of the samples, it can be seen that the assumption of a planar surface is incorrect. Due to this non-planar morphology, the incident light on the sample will refract and transmit through the sample at an

angle, thus increasing the length of its path through the sample. While this is not an issue for thick samples where all light is absorbed within a distance of their thickness, thin samples require a correction. In addition to a requirement for the distance of the first pass of the light to be altered based on the refraction angle, the reflection of the back surface of the wafer also needs to be considered. In thin samples, the high wavelength LEDs will have enough light transmit through the entirety of the wafer such that backside reflections are significant.[50]

These effects were first going to be handled using a modified reflection term in the form of Equation (55). This term has been previously used in modeling to handle back surface reflection in wafers.[35]

$$f_{refl} = \frac{1 + r(\lambda)e^{2\alpha x - 2\alpha w}}{1 - r(\lambda)^2 e^{-2\alpha w}}\left(1 - r(\lambda)\right) \tag{55}$$

Equation (55) is based on the assumption of planar surfaces, however, so the correction was done with a more in depth model. An online tool from PVLighthouse, a wafer ray tracer, was used in order to calculate effective pathlength enhancement factors based on the surface morphologies of the wafers and their widths. This effective pathlength enhancement gave a factor that accounts for all the refraction and reflection within the wafer. This factor is multiplied by the width of the wafer to give an effective width the light travels within the material. This is used in the calculations by changing the bounds on the integration for the generation rate shown in Equation (31).

## 3.4 Measured Wafers and Analytical Model Fits

This study involved the measurement of several silicon wafers. It has been shown that the analytical model given in Section 3.2.2 has been able to fit through the

effective lifetime data gathered for these samples, and information about the bulk lifetime and surface recombination velocity has been extracted from these samples. The samples used in this study include a 1mm thick unpassivated n-type sample, a set of two n-type samples taken from two separate stages of a solar cell production line, and a set of two p-type samples also taken from two separate stages of a cell production line. All five of the samples measured were able to be characterized satisfactorily by the analysis techniques and corrections discussed. As expected, the passivated samples measured had low surface recombination velocities.[51]

### *3.4.1 Unpassivated 1mm thick n-type sample*

The first wafer measured in this study was the thick unpassivated n-type wafer. As this sample was extremely thick when compared to the absorption length coefficients, there were no corrections needed for pathlength enhancement. However, since this sample did require a correction for the trap photoconductance. The nine data points were taken from the LEDs, and are shown below in Figure 24. Also shown in the figure is the analytical model fit. As shown, the fit goes through the data points with a bulk lifetime value of 2.10ms and surface recombination velocity of 10,600cm/s. Note how the bulk lifetime is a couple orders of magnitude higher than the effective lifetimes measured, which is due to the high surface recombination velocity.

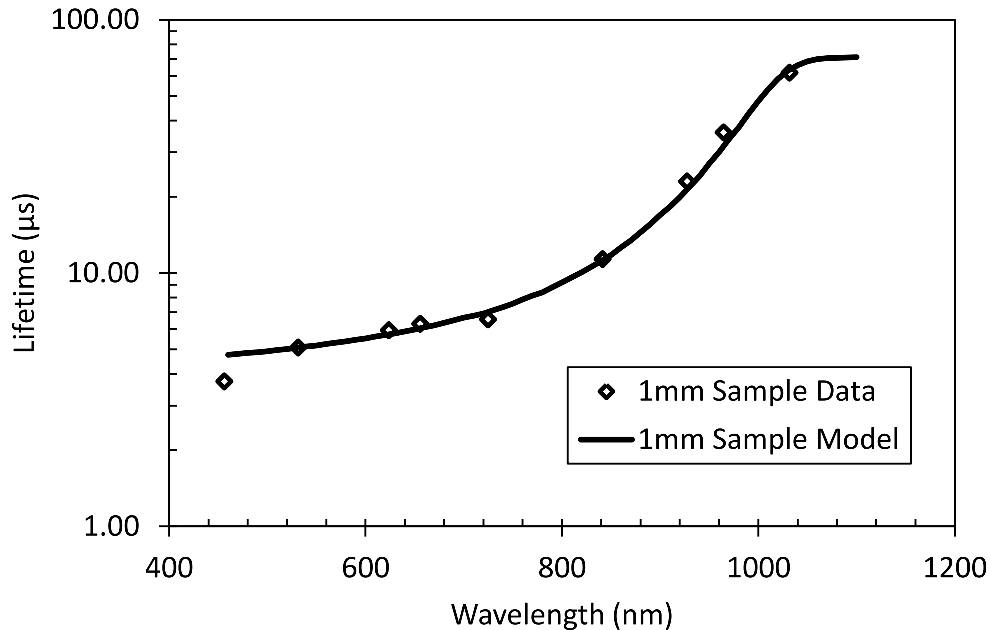


Figure 24: Measured data and analytical model fit for 1mm n-type unpassivated wafer. The analytical model was fit with values of $\tau_b$ = 2.10ms and $S$ = 10,600cm/s.

*3.4.2 Unpassivated and Passivated n-type Wafers*

After characterizing the 1mm sample, the photoconductive lifetime technique was used in order to measure two wafers at separate stages along a PV cell production line. The first of the two wafers came after the bulk silicon was first cut in the wafering process, followed by an isotropic etch method to texturize both the front and back sides for improved light coupling. The second came after a passivation step which included the deposition of an amorphous intrinsic silicon layer and a highly doped amorphous p-type silicon layer. These layers are very thin (60nm when compared to the wafer thickness of 160μm) and are considered to have negligible effects on the conductance of the wafer. The data analysis for these thin wafers included both corrections for the trap photoconductivity and corrections for the pathlength enhancement for the high wavelength LEDs. The measurement and model fit for the data on both of these wafers is shown below in Figure 25. From the fits of

the data the lifetime and surface recombination values for these two wafers are extracted. As expected, the two samples have the same bulk lifetime value but have drastically different surface recombination values. The passivation step reduced the surface recombination by several orders of magnitude to a low value of 5.7cm/s.

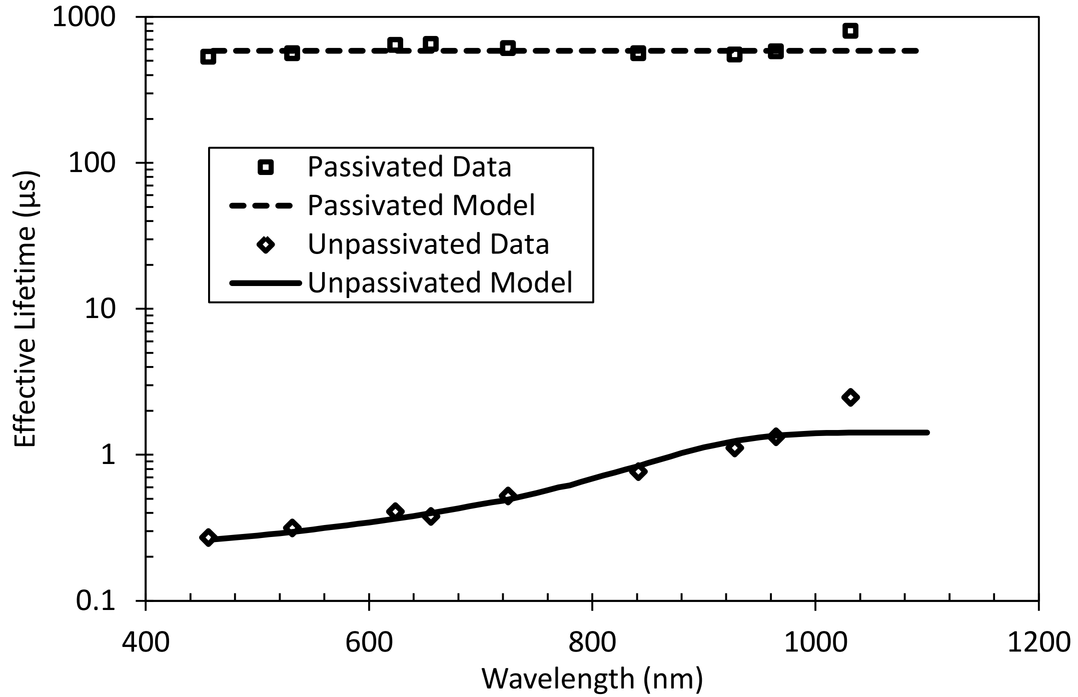


Figure 25: Measured data and analytical model fit for an unpassivated and passivated n-type wafer from the same batch. The model has characteristic values of $\tau_b$ = 1.009ms for both wafers, $S_{pass}$ = 5.7cm/s and $S_{unpass}$ = 33,300cm/s.

### *3.4.3 Unpassivated and Passivated p-type wafers*

In addition to doing this measurement on two stages of a cell with an n-type base, the measurement was also done on two stages of a cell with a p-type base. Once again, the samples were taken from a primary stage after the wafer cutting and texturing process and a secondary stage after a passivation process that included deposition of a thin emitter layer. The data and model fits are shown below in Figure 26. Again, the model reveals a similar lifetime between the two samples and a drastic change in the surface recombination velocity as expected. It is also of note that the measurement

process was able to measure lifetimes below 100ns for the passivated p-type wafer. This was achieved through averaging to detect small photoconductance changes as well as having multiple LEDs of the low wavelength values to increase intensity.

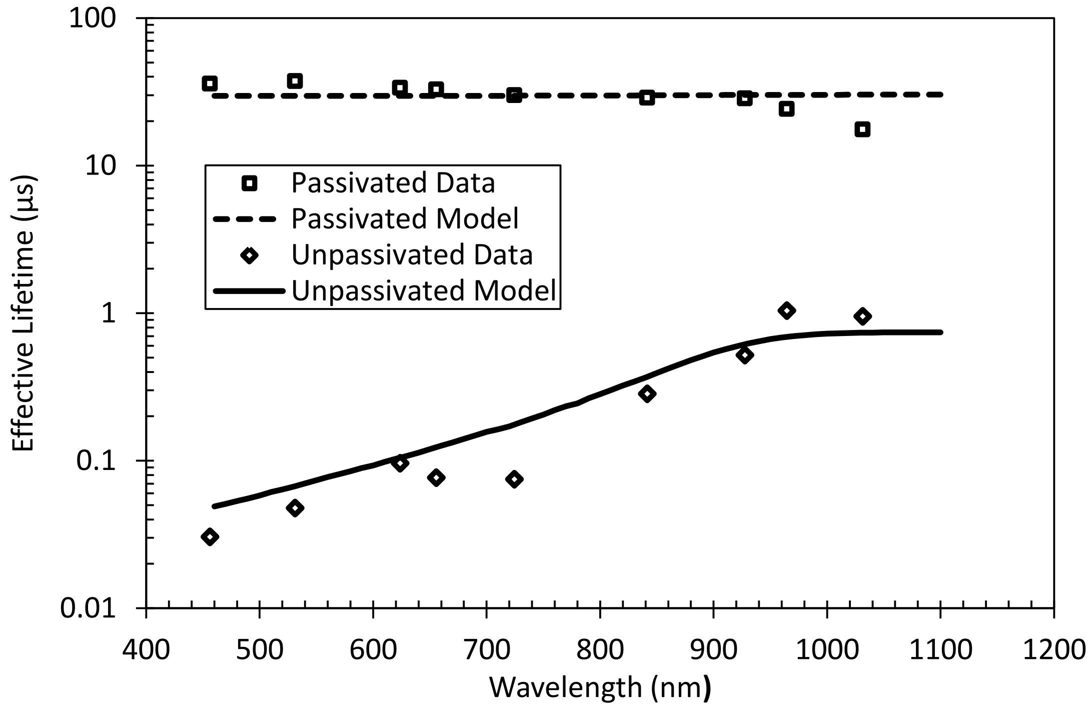


Figure 26: Measured data and analytical model fit for an unpassivated and passivated p-type wafer from the same batch. The model has characteristic values of $\tau_b$ = 0.149ms for both wafers, $S_{pass}$ = 235cm/s and $S_{unpass}$ = 238,000cm/s.

## 3.5 Effects of Excess Carrier Densities

As shown in Section 3.1, the measurements are driven by a sinusoidal input varying from a "dark" or ambient condition to a maximum LED output. This means that the excess carrier densities seen by the wafer can vary greatly over the course of the measurement. It was seen that in the unpassivated samples, the excess carrier density never got to high values that placed the wafer out of the Shockley Read Hall recombination regime, however the passivated samples had a much higher photoconductive response caused by a higher generated excess carrier density. The

lifetimes measured for these passivated samples were excess carrier concentration dependent and are discussed in this section.

The passivated, or stage two, n-type wafer described above had a very large photoconductive response to the input LED signal. This corresponded to a large range of excess carrier densities measured, and it was seen that the charge carrier lifetime was dependent on the excess carrier density. As seen in Figure 27, the lifetimes increased then decreased with increasing excess carrier density. This is due to effects of SRH recombination and emitter recombination. It should also be noted that for the data shown in Section 3.4, the lifetimes were taken at a consistent excess carrier concentration.

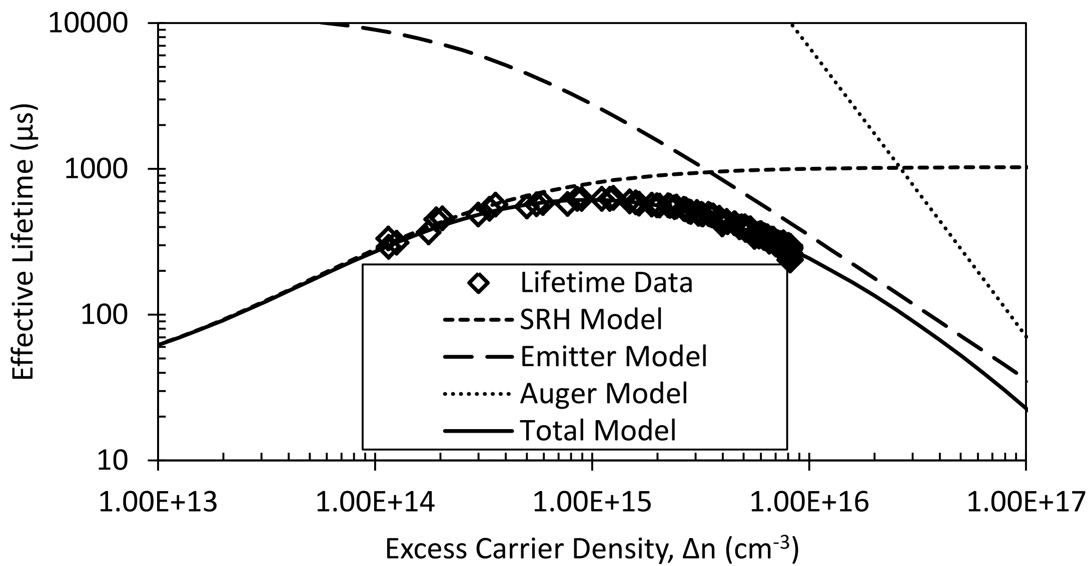


Figure 27: Effective lifetime dependence on excess carrier density for the passivated n-type wafer exposed to the 850nm LED. SRH recombination mechanisms dominate at carrier concentrations below $10^{15}cm^{-3}$ and emitter recombination dominates at concentrations above $10^{15}cm^{-3}$.

The passivated p-type wafer also showed a relationship between excess carrier density and charge carrier lifetime. As with the n-type wafer, the lifetime data used in the analysis in Section 3.4 was taken at a consistent excess carrier concentration.

# Conclusions

Through this study, it has been shown that values relating to the carrier transport in silicon can be extracted using a quasi-steady state contactless technique. Through the wavelength-dependent photoconductivity measurements of wafers before and after a passivation process, the reduction of surface recombination velocity can be seen.

The measurement apparatus developed for this measurement allowed for charge carrier excitation with a narrow bandwidth wavelength signal. Using this apparatus, the spectral dependence of the measurement was used to extract bulk lifetime and surface recombination velocity. Though the power from the incident LEDs was not as intense as other input sources, a good measurement of the lifetime was attainable through averaging on a periodic input signal. The LEDs, when paired with the coupled light guide, were also able to provide the large uniformly lit area required by the coil measurement.

Since this measurement is an aggregate measurement of the properties of a wafer, the specific carrier densities cannot be measured as a function of depth into the wafer, however this depth dependence can be modeled using the diffusion equation and boundary conditions shown. The strength of the RF coil measurement lies in the measurement being done under quasi-steady state conditions which are most similar to the conditions a finished PV cell would encounter when in use.

Because the developed system was able to measure carrier lifetimes down to the 30 ns range, this technique can be further used to measure other photovoltaic materials such as gallium arsenide and other III-V materials.

# Bibliography

[1] Y. Arafat, F. M. Mohammedy, and M. M. Shahidul Hassan, “Optical and Other Measurement Techniques of Carrier Lifetime in Semiconductors,” *Int. J. Optoelectron. Eng.*, vol. 2, no. 2, pp. 5–11, 2012.

[2] D. K. Schröder, “Carrier lifetimes in silicon,” *IEEE Trans. Electron Devices*, vol. 44, no. 1, pp. 160–170, 1997.

[3] C. Berge, J. Schmidt, B. Lenkeit, H. Nagel, and A. G. Aberle, “Comparison of effective carrier lifetimes in silicon determined by transient and quasi-steady-state photoconductance measurements,” *2nd World Conf. Exhib. Photovolt. Sol. Energy Convers.*, no. JULY, pp. 1426–1429, 1998.

[4] W. M. Bullis and H. R. Huff, “Interpretation of Carrier Recombination Lifetime and Diffusion Length Measurements in Silicon,” *J. Electrochem. Soc.*, vol. 143, no. 4, pp. 1399–1405, 1996.

[5] M. A. Afromowitz and M. Didomenico, “Measurement of free-carrier lifetimes in GaP by photoinduced modulation of infrared absorption,” *J. Appl. Phys.*, vol. 42, no. 8, pp. 3205–3208, 1971.

[6] Z. G. Ling and P. K. Ajmera, “Measurement of bulk lifetime and surface recombination velocity by infrared absorption due to pulsed optical excitation,” *J. Appl. Phys.*, vol. 69, no. 1, pp. 519–521, 1991.

[7] K. L. Luke and L. J. Cheng, “Analysis of the interaction of a laser pulse with a silicon wafer: Determination of bulk lifetime and surface recombination velocity,” *J. Appl. Phys.*, vol. 61, no. 6, pp. 2282–2293, 1987.

[8] J. A. Mroczkowski, “Lifetime measurement in Hg0.7Cd0.3Te by population

modulation," *Appl. Phys. Lett.*, vol. 38, no. 4, p. 261, 1981.

[9] R. J. Kumar, J. M. Borrego, R. J. Gutmann, J. R. Jenny, D. P. Malta, H. M. Hobgood, and C. H. Carter, "Microwave photoconductivity decay characterization of high-purity 4H-SiC substrates," *J. Appl. Phys.*, vol. 102, no. 1, 2007.

[10] T. Otaredian, "Separate contactless measurement of the bulk lifetime and the surface recombination velocity by the harmonic optical generation of the excess carriers," *Solid State Electron.*, vol. 36, no. 2, pp. 153–162, 1993.

[11] O. Palais and A. Arcari, "Contactless measurement of bulk lifetime and surface recombination velocity in silicon wafers," *J. Appl. Phys.*, vol. 93, no. 8, pp. 4686–4690, 2003.

[12] M. Turek, "Interplay of bulk and surface properties for steady-state measurements of minority carrier lifetimes," *J. Appl. Phys.*, vol. 111, no. 12, p. 123703, 2012.

[13] R. a. Sinton, "Practical measurement of bulk lifetime and surface recombination by using wavelength dependence," *3rd World Conf. onPhotovoltaic Energy Conversion, 2003. Proc.*, vol. 1, pp. 951–954, 2003.

[14] C. Kittel, *Introduction to Solid State Physics*, 8th ed. John Wiley & Sons, Inc., 2005.

[15] D. A. Neamen, *Semiconductor Physics and Devices: Basic Principles*, 4th ed. New York, NY: McGraw-Hill, 2012.

[16] S. O. Kasap, *Principles of Electronic Materials and Devices*, 3rd ed. New York, NY: McGraw-Hill, 2006.

[17] S. M. Sze and K. K. Ng, *Physics of Semiconductor Devices*. 2007.

[18] B. G. Streetman, *Solid State Electronic Devices*, 2nd ed. Englewood Cliffs, N.J.: Prentice-Hall, Inc., 1980.

[19] W. Warta, “Advanced defect and impurity diagnostics in silicon based on carrier lifetime measurements,” *Phys. Status Solidi Appl. Mater. Sci.*, vol. 203, no. 4, pp. 732–746, 2006.

[20] S. Rein, T. Rehrl, W. Warta, and S. W. Glunz, “Lifetime spectroscopy for defect characterization: Systematic analysis of the possibilities and restrictions,” *J. Appl. Phys.*, vol. 91, no. 3, pp. 2059–2070, 2002.

[21] W. Shockley and W. T. Read, “Statistics of the Recombination of Holes and Electrons,” *Phys. Rev.*, vol. 87, no. 46, pp. 835–842, 1952.

[22] R. N. Hall, “Electron-Hole Recombination in Germanium,” *Phys. Rev.*, vol. 175, no. 3, p. 387, 1968.

[23] D. Macdonald, A. Cuevas, M. Stocks, M. Kerr, and C. Samundsett, “Recombination and trapping in multicrystalline silicon,” 1999.

[24] A. Richter, S. W. Glunz, F. Werner, J. Schmidt, and A. Cuevas, “Improved quantitative description of Auger recombination in crystalline silicon,” *Phys. Rev. B - Condens. Matter Mater. Phys.*, vol. 86, no. 16, pp. 1–14, 2012.

[25] A. Richter, F. Werner, A. Cuevas, J. Schmidt, and S. W. Glunz, “Improved parameterization of Auger recombination in silicon,” *Energy Procedia*, vol. 27, pp. 88–94, 2012.

[26] M. J. Kerr and A. Cuevas, “General parameterization of Auger recombination in crystalline silicon,” *J. Appl. Phys.*, vol. 91, no. 3, pp. 2473–2480, 2002.

[27] T. Trupke, M. A. Green, P. Würfel, P. P. Altermatt, A. Wang, J. Zhao, and R. Corkish, "Temperature dependence of the radiative recombination coefficient of intrinsic crystalline silicon," *J. Appl. Phys.*, vol. 94, no. 8, pp. 4930–4937, 2003.

[28] A. G. Aberle, "Surface passivation of crystalline silicon solar cells: a review," *Prog. Photovoltaics Res. Appl.*, vol. 8, no. 5, pp. 473–487, 2000.

[29] M. J. Kerr and a Cuevas, "Very low bulk and surface recombination in oxidized silicon wafers," *Semicond. Sci. Technol.*, vol. 17, no. 1, pp. 35–38, 2002.

[30] R. R. King, R. A. Sinton, and R. M. Swanson, "Studies of Diffused Phosphorus Emitters: Saturation Current, Surface Recombination Velocity, and Quantum Efficiency," *IEEE Trans. Electron Devices*, vol. 37, no. 2, pp. 365–371, 1990.

[31] M. J. Kerr, J. Schmidt, A. Cuevas, and J. H. Bultman, "Surface recombination velocity of phosphorus-diffused silicon solar cell emitters passivated with plasma enhanced chemical vapor deposited silicon nitride and thermal silicon oxide," *J. Appl. Phys.*, vol. 89, no. 7, pp. 3821–3826, 2001.

[32] E. Yablonovitch and T. Gmitter, "Auger recombination in silicon at low carrier densities," *Appl. Phys. Lett.*, vol. 49, no. 10, pp. 587–589, 1986.

[33] B. Fischer, "Loss Analysis of Crystalline Silicon Solar Cells Using Photoconductance and Quantum Efficiency Measurements," 2003.

[34] A. Cuevas, "The effect of emitter recombination on the effective lifetime of silicon wafers," *Sol. Energy Mater. Sol. Cells*, vol. 57, no. 3, pp. 277–290,

1999.

[35] M. Bail and R. Brendel, "Separation of Bulk and Surface Recombination By Steady State Photo Conductance Measurements," *16th Eur. Photovolt. Sol. Energy Conf.*, no. May, pp. 1–5, 2000.

[36] C. Honsberg and S. Bowden, "Photovoltaic Education Network," 2013. [Online]. Available: http://www.pveducation.org/pvcdrom. [Accessed: 20-Jun-2004].

[37] R. Sinton and T. Mankad, "Contactless Carrier-Lifetime Measurement in Silicon Wafers, Ingots, and Blocks," pp. 1–14, 2010.

[38] M. C. Chen, "Sensitive contactless eddy-current conductivity measurements on Si and HgCdTe," *Rev. Sci. Instrum.*, vol. 60, no. 6, pp. 1116–1122, 1989.

[39] M. Gruber, "Characterization of ingots and wafers for photovoltaic applications," no. August, 2012.

[40] G. L. Miller, D. A. H. Robinson, and J. D. Wiley, "Contactless measurement of semiconductor conductivity by radio frequency-free-carrier power absorption," *Rev. Sci. Instrum.*, vol. 47, no. 7, pp. 799–805, 1976.

[41] R. A. Sinton, A. Cuevas, and M. Stuckings, "Quasi-Steady-State Photoconductance, a new method for Solar Cell Material and Device Characterization," *25th PVSC*, pp. 457–460, 1996.

[42] J. S. Swirhun, M. K. Forsyth, T. Mankad, and R. A. Sinton, "Contactless Measurement of Carrier Lifetime on Silicon Ingots and Bricks James S. Swirhun, M. Keith Forsyth, Tanaya Mankad, and Ronald A. Sinton Sinton Instruments, Boulder, CO 80301 USA," vol. 1210, 2010.

[43] S. K. Pang and A. Rohatgi, “A new methodology for separating Shockley-Read-Hall lifetime and Auger recombination coefficients from the photoconductivity decay technique,” *J. Appl. Phys.*, vol. 74, no. 9, pp. 5554–5560, 1993.

[44] S. Bowden and R. A. Sinton, “Determining lifetime in silicon blocks and wafers with accurate expressions for carrier density,” *J. Appl. Phys.*, vol. 102, no. 12, 2007.

[45] R. a Sinton, T. Mankad, S. Bowden, and N. Enjalbert, “Evaluating silicon block and ingots with quasi-steady-state lifetime measurements,” *Proc. 19th Eur. Photovolt. Sol. Energy Conf. , Paris, Fr.*, pp. 520–523, 2004.

[46] G. S. Kousik, Z. G. Ling, and P. K. Ajmera, “Nondestructive technique to measure bulk lifetime and surface recombination velocities at the two surfaces by infrared absorption due to pulsed optical excitation,” *J. Appl. Phys.*, vol. 72, no. 1, pp. 141–146, 1992.

[47] Y.-I. Ogita, “Bulk lifetime and surface recombination velocity measurement method in semiconductor wafers,” *J. Appl. Phys.*, vol. 79, no. 9, p. 6954, 1996.

[48] M. Turek, C. Möller, and K. Lauer, “Investigation of excess charge carrier lifetime measurements on samples of arbitrary thickness,” *27th Eur. Photovolt. Sol. Energy Conf. Exhib.*, pp. 1045–1048, 2012.

[49] D. Macdonald, R. A. Sinton, and A. Cuevas, “On the use of a bias-light correction for trapping effects in photoconductance-based lifetime measurements of silicon,” *J. Appl. Phys.*, vol. 89, no. 5, pp. 2772–2778, 2001.

[50] L. Zeng, Y. Yi, C. Hong, J. Liu, N. Feng, X. Duan, L. C. Kimerling, and B. A.

Alamariu, "Efficiency enhancement in Si solar cells by textured photonic crystal back reflector," *Appl. Phys. Lett.*, vol. 89, no. 11, pp. 11–14, 2006.

[51] E. Yablonovitch, D. L. Allara, C. C. Chang, T. Gmitter, and T. B. Bright, "Unusually low surface-recombination velocity on silicon and germanium surfaces," *Phys. Rev. Lett.*, vol. 57, no. 2, pp. 249–252, 1986.